The Effect of the Interstitial Flow on the Directional Cell Migration and Sprouting of Capillaries

by

Chen-rei Wan
S.B Mechanical Engineering
S.B Biomedical Engineering
Carnegie Mellon University, 2005

SUBMITTED TO THE DEPARTMENT OF MECHANICAL ENGINEERING IN PARTIAL FULFILLMENT OF THE REQUIREMENTS FOR THE DEGREE OF

MASTER OF SCIENCE IN MECHANICAL ENGINEERING AT THE MASSACHUSETTES INSTITUTE OF TECHNOLOGY

JUNE 2007

Signature of the Author .....
Department of Mechanical Engineering
May 17, 2007

Certified by .....
Roger Kamm
Professor of Mechanical Engineering and Biological Engineering
Thesis Supervisor

Accepted by .....
Lallit Anand
Chair, Department Committee on Graduate Students
Department of Mechanical Engineering

This page is intentionally left blank

The Effect of the Interstitial Flow on the Directional Cell Migration and Sprouting of Capillaries

by

Chen-rei Wan

Submitted to the Department of Mechanical Engineering on May 20th, 2007 in Partial Fulfillment of the Requirements for the Degree of Master of Science in Mechanical Engineering

Abstract

Development of functional endothelium in tissue engineering is both critical and challenging. It is critical because of its role in transporting nutrient and waste in tissues larger than the length scale of diffusion. It is challenging because of its complexity in both the chemical and mechanical environments actively evolving in both space and time. In addition to the signals from the microenvironment, cells are more than likely to receive global signaling as well. The goal of the overall project is to establish a functional endothelium for a long period of time under the optimal chemical and physical conditions.

This master's thesis project focuses specifically on the effect of interstitial fluid flow on the capillary morphogenesis process. Interstitial fluid flow is defined as flow perpendicular to the endothelial monolayer, as opposed to shear flow which is parallel. Interstitial flow is an essential process *in vivo* both in normal physiology and pathology. Liver filtration system, angiogenesis during wound healing, vasculogenesis during fetal development and lymphoangiogenesis are a few examples that depend heavily on interstitial flow. Pathologically, interstitial flow is observed when the vessels are abnormally leaky, such as the case in tumor-induced angiogenesis.

In vivo observations of angiogenesis suggest the nascent blood vessels sprout from the venous end. This indicates that the interstitial flow direction is opposite of the direction of sprouting. *In vitro* studies of interstitial flow on endothelial cells are not done until the recent development of three dimensional culture systems. The studies suggest that capillary branching is biased the direction of interstitial flow when VEGF is matrix-bound. The seemingly contradicting results ignite our interest in investigating whether the direction of interstitial flow has an impact on the directional migration or sprouting of endothelial cells or not in a device-independent method *in vitro*.

Two different designs of 3D culture bioreactors were used, one in the millimeter scale while the other one in micrometer scale. In the meso-scale bioreactor, the endothelial cells appeared to migrate and sprout against the flow direction. This result is consistent whether cells were seeded as a monolayer or suspended in collagen gel. This finding seemed to be opposite from the current *in vitro* findings in the literature. Therefore, another device was used to examine the same problem in attempt to eliminate the artifacts of a certain device. In the microfluidic device, no consistent correlation was found between the direction of flow and the extent of cell migration and capillary morphogenesis. Extension gel contraction was observed which made the analysis more difficult and the assumption of interstitial flow through the collagen gel in the device less valid. Multiple endothelial cell monolayers were observed migrating on the gel

surface and the 3D reconstruction images suggest possible connections between the monolayer forming complex 3D networks.

This project examined the two three-dimensional culture systems allowing endothelial cell invasion and migration. Although the results didn't align for the two devices, it raised an interesting question of the device-dependency when studying capillary morphogenesis. The different scales can create a different chemical and mechanical environment which changes the relative importance between diffusion and convection. From first-order modeling, it can be seen that the presence of interstitial flow can have a drastic influence on the endogenous concentration of chemicals although the corresponding cell migration behavior was not observed experimentally. Therefore, the definitive answer of the effect of interstitial flow on capillary morphogenesis is still open to debate. To truly investigate the effect of interstitial flow on the directional cell migration and sprouting, more attention needs to be paid toward understanding the relative importance of diffusion and migration in the specific experimental setup.

Thesis Supervisor: Roger Kamm
Title: Professor of Mechanical Engineering and Biological Engineering

Acknowledgements

I would like to thank, first and foremost, my research advisor, Roger Kamm, for his guidance to consider the holistic picture of the research topic and also his patience and understanding when research was going less than optimal. I would also like to express my deepest appreciation to Carlos Semino who assisted me in countless ways, from understanding cell biology, experimental techniques to interesting Spanish phrases.

I would also like to thank all students and postdocs who have helped me along the way to transform me from a cell biology illiterate to someone who truly appreciates the complexity and beauty of biology:
Alisha Sieminiski for introducing me to cell culture and explaining PATIENTLY of the basic principles,
Rodrigo Hernandez for teaching me how to use the meso-scaled bioreactors,
Sid Cheng for introducing me to microfluidic devices,
Ryo Sudo for his generosity of sharing useful experimental technique tips,
Aida Rahim, Anusuya Das, Nathan Hammond, Hyungsuk Lee, Taeyoon Kim and the rest of the Kamm lab members for being great labmates and keeping me company.

I would also like to thank my family who supported me every step along the way.

This work is supported in part by a National Science Foundation Graduate Fellowship.

This page is left intentionally blank

List of Contents

ABSTRACT 3

ACKNOWLEDGEMENTS 5

LIST OF CONTENTS 7

LIST OF FIGURES 9

LIST OF EQUATIONS 11

1. BACKGROUND 13

1.1. Tissue Engineering: Vascularization 13
1.1.2 Vasculogenesis 13
1.1.3 Angiogenesis 14
1.1.3.1 *In Vivo* Observations of Angiogenesis 15
1.1.3.2 *In Vitro* Observations of Angiogenesis 15

1.2. Mechanobiology of Vascularization 17
1.2.1 Fluid Flow 18
1.2.1.1 Shear Flow 18
1.2.1.2 Interstitial Flow 19

1.3 Development of Meso-scale Bioreactor 20

1.4 Development of Microfluidic Device 22

2. OBJECTIVE 23

3. METHODS 24

3.1 Cell Culture 24

3.2 Meso-Scale Bioreactor 24
3.2.1 Device Dimensions 24
3.2.2 Gel Loading 25
3.2.3 Cell Loading 26
3.2.4 Flow Induction 27

3.3 Microfluidic Devices 28
3.3.1 Device Dimension 29
3.3.2 Device Production and Preparation 30
3.3.3 Gel Loading 30
3.3.4 Cell Loading 31
3.3.5 Flow Induction 32

3.4 Flow Velocity and Permeability Calculations 32

3.5 Image Acquisition and Analysis 34

4. RESULTS 35

4.1 Meso-scale Bioreactors 35
4.1.1 Capillary Morphogenesis from Endothelial Cell Monolayer 36
4.1.2 Capillary Morphogenesis from Endothelial Cell Monolayer Sandwiched between Collagen Scaffolds 37
4.1.3 Capillary Morphogenesis from Suspended Cells in Collagen 40

4.2 Microfluidic Device 44
4.2.1 Capillary Morphogenesis from Endothelial Cell Monolayer 45
4.2.2 Extent of Cell Migration 46
4.2.3 Formation of Multiple Monolayers 47
4.2.4 Formation of Connections between Monolayers 50
4.2.5 Time Progression of Network 55

4.3 Two-Tiered Modeling 58
4.3.1 Cellular Level Modeling 58
4.3.1.1. Mechanical Stress on the Endothelial Cell Wall 58
4.3.1.2 First Order Transport Phenomenon in between the Interendothelial Cleft Space 60
4.3.2 Bioreactor Scale Modeling 62

5. DISCUSSION 65

5.1 Meso-Scale Bioreactor 65
5.1.1 Effect of Flow 66
5.1.1.1 Effect of Magnitude of Velocity 66
5.1.1.2 Effect of Direction of Flow 67
5.1.2 Effect of Growth Factors/Serum 69
5.1.3 Effect of Cell Seeding Density 70

5.2 Microfluidic Device 70
5.2.1 Effect of Direction of Flow 71
5.2.2 Formation of Multiple Monolayers 74
5.2.3 Connections between Monolayers 75

5.3 Comparison of the Two Devices 76

5.4 Modeling 77

6 CONCLUSION 80

APPENDICES 82

Appendix I : Protocol of Microfluidic Device Setup 82

Appendix II : MathCad Code for First Order Model 84

REFERENCES 89

List of Figures

Figure 1: Capillary Morphogenesis with/without Flow 21
Figure 2: Baseline results from Microfluidic Device 22
Figure 3: Meso-Scale Bioreactor Design 25
Figure 4: Flow Circuit for Meso-scale Bioreactor 28
Figure 5: Microfluidic Device *Figure 6: Gel Cage of the Microfluidic Device* 29
Figure 7: Schematic Drawing of the final setup of the Microfluidic Device 32
Figure 8: Schematic Drawing of the Gel Cage 33
Figure 9: Schematics of Three Different Experimental Setups 35
Figure 10: Sprouting from Monolayer at Two Different Time Points 36
Figure 11: Ring-shaped Reorganization of Endothelial Cell Monolayer 37
Figure 12: Sprouts Observed in High Flow Velocity Experiments 38
Figure 13: Quantitative Analysis of Sprouts under 50μm/min Flow 39
Figure 14: Quantitiave Analysis of Sprouts under 73 μm/min Flow 40
Figure 15: Internal Network Formation of Suspended Cells under Static Culture 42
Figure 16: Effect of VEGF on Internal Cell Network 42
Figure 17: Effect of Flow on Internal Network of Suspended Cells 43
Figure 18: Invasion into the Acelluar Collagen Layers 44
Figure 19: Sprouting in Microfluidic Device 46
Figure 20: Extent of Cell Migration in the Microfluidic Device 47
Figure 21: Fluorescent Images of the Endothelial Cell Migration: Formation of Multiple Monolayers 50
Figure 22: Connection between Two Monolayers 51
Figure 23: Reconstructed 3D Deconvolution Images of the Cell Network 52
Figure 24: Deconvulated 2D Images of Actin Structure 55
Figure 25: Temporal Progression of Cell Migration 56
Figure 26: Average Invasion Area over Time 57
Figure 27: Average Maximal Invasion Length over Time 57
Figure 28: Schematic of the Transport in the Interendothelial Cleft Space (Not Drawn to Scale) 60
Figure 29: Concentration Profile in the Interendothelial Cleft Space with Shedding 62
Figure 30: Concentration Distribution in Gel in Meso-scale Bioreactor with Shedding 63
Figure 31: Concentration Distribution in the Microfluidic Device with Growth Factors Shedded from Cells 64
Figure 32: Schematic of Small Gaps in between Gel and Device 71
Figure 33: Extent of Gel Contraction from Two Different Suppliers 74
Figure 34: Deterioation of the Sample over Time 75

This page is left intentionally blank

List of Equations

Equation 1: Effective Cross-sectional Area 33
Equation 2: Flow Velocity of the Microfluidic Device 33
Equation 3: Darcy's Law 33
Equation 4: Rearranged Form of Darcy's Law to Calculate Permeability 33
Equation 5: Hydraulic Conductivity of the 2mg/ml Collagen Gel in the Microfluidic Device 34
Equation 6: Velocity Profile in the Interendothelial Cleft Space 59
Equation 7: Pressure Difference between the two Ends of the Cleft Space 59
Equation 8: Shear Stress along the Wall of the Cell 59
Equation 9: Governing Equation of the Transport in the Interendothelial Cleft Space 61
Equation 10: Governing Equation of the Transport in the Gel 62

This page is left intentionally blank

1. Background

1.1. Tissue Engineering: Vascularization

For the past two decades, the field of tissue engineering has become one of the most promising answers to the question of replacements of dysfunctional tissues. It was first defined in 1987 by the National Science Foundation as "an interdisciplinary field that applies the principles of engineering and the life sciences towards the development of biological substitutes that restore, maintain or improve tissue functions." [1] To restore the functionality of large tissues or organs requires proper vascularization which provides sufficient nutrient and waste transport. This remains to be one of the biggest challenges today. Because of the lack of success in developing functional vascular network, current tissue engineering is limited to avascular tissues, such as cartilage, or micro-scaled culture. A main focus of tissue engineering has, therefore, been developing capillary networks *in vitro* to mimic the *in vivo* phenomenon. There are two types of vascular formations in three dimensions, vasculogenesis and angiogenesis, which will be discussed in further details.

1.1.2 Vasculogenesis

Vasculogenesis describes the growth of the primary vascular plexus and the differentiation of the angioblasts into endothelial cells. It is the first step in the development of the circulatory system in vertebrates. [2-4] Most *in vivo* studies on vasculogenesis are done on yolk sac or embryos. In vitro models have also been developed. The high level of VEGF release and

the high-affinity binding of VEGF receptor, Tie-2 are observed in the initial stage of vascuologenesis and responsible for transforming the mesoderm into blood islands and eventual primary plexus. [5, 6] Endothelial cells or hematopoietic cells can be induced and differentiated in vitro by the stimulation of FGF. [7]. After the primary plexus is formed in 3D, it is followed by a remodeling process, angiogenesis, which forms nascent vessels from the preexisting ones or induces regression of the unwanted vessels.

1.1.3 Angiogenesis

In the developmental stage, vasculogenesis is followed by angiogenesis which remodels the primary network. Angiogenesis, the formation of new blood vessels from pre-existing ones, also plays crucial roles in adulthood in normal physiological phenomenon such as wound healing, ovarian follicle maturation cycles and pathological scenarios such as tumor growth and retina occlusions. [2, 8-10] Folkman first discovered that inhibiting angiogenesis is an effective method in slowing down growth of numerous types of solid tumors.[11] Angiogenesis was discovered in the beginning of the 1900's. It was observed clearly for the first time in the late 1920's when the Clarks introduced the transparent chamber.[12] Despite the early discovery, the first systematic approach in observing the angiogenesis process, especially in the context of tumor growth, was performed by Judah Folkman who did extensive work both *in vivo* and *in vitro*. [11, 13, 14]

1.1.3.1 *In Vivo* Observations of Angiogenesis

Ausprunk and Folkman implanted V2 carcinoma in rabbit cornea in 1976 to observe tumor-induced angiogenesis.[14] Several key findings are as follows:

1. by the second day of the implantation, endothelial cells emigrated from preformed vessels toward the tumor implant;
2. cell-cell junctions were loosened and new lumina appreared in the walls of the existing venules by the second day;
3. capillary sprouts were first observed histologically after 4 days;
4. cell migration appeared to loosen the cell-cell junctions. As a result, cells proliferation occured. The process was observed near the distal tip of the capillary sprout; and
5. once the new vessels were formed, these tumor-induced vessels displayed similar characteristics to wound-induced capillaries.

This study was one of the first systematic descriptions of the angiogenesis process *in vivo*. Even though this study was done over 30 years ago, these key finding still prove to be invaluable in our understanding of angiogenesis *in vivo*.

1.1.3.2 *In Vitro* Observations of Angiogenesis

Although the *in vivo* model of angiogenesis mimics more closely to what happens physiologically, it is often entangled with other complex phenomenon, such as blood coagulation, which obstructs the direct observations. Therefore, *in vitro* models have been developed over the years to investigate the angiogenesis process in a much more controlled

environment. The first *in vitro* experiment to study angiogenesis of capillary endothelial cells was done in 1980 by Folkman and Haudenschild. [11] In this study, capillary endothelial cells were cultured with tumor-conditioned media in gelatin-coated plates. One of the important findings in this study was the fact that all the information required for capillary formation resided in one type of cells, endothelial cells. It also found that the rate of capillary endothelial cell migration was correlated with the concentration of tumor-conditioned media. This study established the significance and practicality of *in vitro* models of angiogenesis.

Over the years, the *in vitro* experiments have improved drastically to better model the angiogenesis process physiologically.[15] Because of the advancement of the *in vitro* models, different growth factors and enzymes related to angiogenesis were isolated and characterized.[16-22] In addition to the discovery of chemical factors, the interactions between endothelial cells and the matrix were also better understood. [18, 23-26] The development of three-dimensional culture systems led researchers into new territories in the investigation of angiogenesis.[27-30] Although different groups take different approaches, the general concept to a three-dimensional *in vitro* model is similar. Cells are seeded either on the surface of or embedded within a scaffolding material which mimics the extracellular matrix and gives support to the system. Cells attach to the matrix through focal adhesion complexes. The interaction between cells and the environment goes in both directions. As cells migrate and/or proliferate, they release matrix metalloproteinases (MMP's) which degrade the scaffolding material allowing invasion. On the other hand, the matrix and the

chemical environment also influence the cell decision-making process. [10, 31] The matrix properties, both physically and chemically, impact cell behaviors greatly. The process of chemotaxis (migration due to chemical gradient), haptotaxis (migration due to gradient of adhesion sites to the extracellular matrix) and differential cell migration due to varying scaffold stiffness are all examples of how the physical and chemical environment influences cell behaviors.

1.2. Mechanobiology of Vascularization

Not only do the different growth factors and the scaffold properties play an important role in angiogenesis, mechanical forces have also been demonstrated to be crucial.[32, 33] It is not surprising that mechanical forces, such as shear stresses [34-36], pressure or cyclic stretch [37, 38], have an effect on angiogenesis since these forces are present and highly dynamic physiologically. The field of mechanobiology emerged over twenty years ago.[39] Mechanobiology/mechanotransduction recently received much attention demonstrating its richness and complexity.[40, 41] Briefly, the basic concept of mechanobiology is that mechanical forces are transmitted to the cells from the external environment via focal adhesion complexes. These forces are transmitted through the cytoskeleton of the cell which may activate chemical processes within the cell. The transition of mechanical forces to chemical signals has been proven to be important in angiogenesis.[41] In the following section, I will focus on the effect of fluid flow, both in the shear flow and interstitial flow.

1.2.1 Fluid Flow

One of the mechanical forces on endothelial cells is applied in the form of fluid flow. Fluid can either flow over the monolayer or through the monolayer. The flow which flows parallel to the monolayer will be referred to as shear flow, and that which flows perpendicular to the monolayer will be referred to as interstitial flow.

1.2.1.1 Shear Flow

Most of the experiments have focused on the effect of shear flow on endothelial cells. This might be because of the limitation of 2D culture. Cells are found to align with the shear flow. A detailed review of the effect of shear flow on endothelial cells was done by Shu Chien et. al.. [42, 43] Several key findings are described below.

Hemodynamic forces are present in blood vessels. The tangential component of it imposes shear stress on the vessel wall composed of a layer of endothelial cells. The effect of shear stress is a highly-complex process. I will focus on the main phenomeonological effects of shear stress on endothelial cells, instead of discussing the details of the changes or activation in signaling pathways. For cell proliferations, the endothelial cell monolayer is stabilized and the cell turnover rate is reduced under steady, unidirectional laminar flow. While under disturbed flow (either turbulent or complex laminar flow as found in regions of bifurcation or complex geometry), cells proliferate in a much higher rate with a sustained phosphorylation of ERK. By the same token, laminar flow acts as a protective mechanism reducing the endothelial cell apoptotic rate. Endothelial cell migration is enhanced by laminar shear flow, but not disturbed flow. Most of these experiments are carried out with

cells plated on a two dimensional surface. Therefore, it is hypothesized that the enhancement of cell migration under laminar flow is related to the increased activity of the lamellipodia.

Cells have been found to align with the direction of the shear flow. This occurs simultaneously with the reorganization of the microfilaments and microtubules. By 12 hours of laminar shear, the cells elongate and rearrange to align with the flow. Shear flow has also been described to increase the cell stiffness. However, there have been discrepancies whether the increase in stiffness can still be sustainted after 24hours. [44, 45]

1.2.1.2 Interstitial Flow

Despite of the fact that shear flow has been studied extensively, interstitial flow has not received as much attention until recently. Interstitial flow is highly relevant to numerous physiological phenomena, angiogenesis during wound healing, vascolugenesis during development or liver filtration functions. [46] Several research groups, including ours, have developed three dimensional *in vitro* models to study interstitial flow. Swartz et. al. have developed a flow system which interstitial flow is generated and flown outward.[47, 48] Fibroblasts were embedded inside the collagen scaffold. With the stimulation of PMA, the experiment indicated that fibroblasts tended to align perpendicular to the flow. The same device was also used to study angiogenesis and lymphogenesis. [49-51]. One of the first studies demonstrated that fibroblast align perpendicular to the flow direction. [52] Suspended fibroblasts inside fibrin matrix were aligned in the circumferential direction when radial flow is applied.

In other studies, VEGF-121 was bonded to the matrix via a MMP-cleavable site and either blood endothelial cells (BEC) or lymphatic endothelial cells (LEC) were suspended inside the gel. Different responses from BECs and LECs were recorded. Under a low interstitial flow (~10 μ m/s), LECs tended to form large vacuoles while BECs tended to form branched networks. [53] Furthermore, in a different study, they found that LECs showed the most extensive organization seeded in a stiffer fibrin matrix and BECs formed most networks when seeded inside a compliant collagen gel. [46] From these different studies, they demonstrated that LECs and BECs may respond to interstitial flow differently.

Helm et. al. looked into how the interstitial flow may induce a concentration gradient when growth factor is tethered to the matrix via MMP-cleavable bonds. They demonstrated the possibility of a gradient both through experiment and simulation. [54, 55]. When growth factors are tethered to matrix and released as proteolyzed by cells, a strong gradient can be created along the direction of the interstitial flow. In experiments, a synergistic effect was observed when VEGF and low level of interstitial flow are both present in the system. The branching of endothelial cells was biased toward the direction of the flow which was clearly due to the autologous morphogen gradient.

1.3 Development of Meso-scale Bioreactor

Rodrigo Hernandez and Carlos Semino designed and fabricated a novel bioreactor with PDMS which allows observation of capillary morphogenesis process with interstitial flow application. In addition to designing the device, Rodrigo also did several experiments to understand how

the magnitude of the flow velocity had an impact on the capillary morphogenesis process. He found that the capillary morphogenesis was most active when interstitial flow was present (Fig. 1).

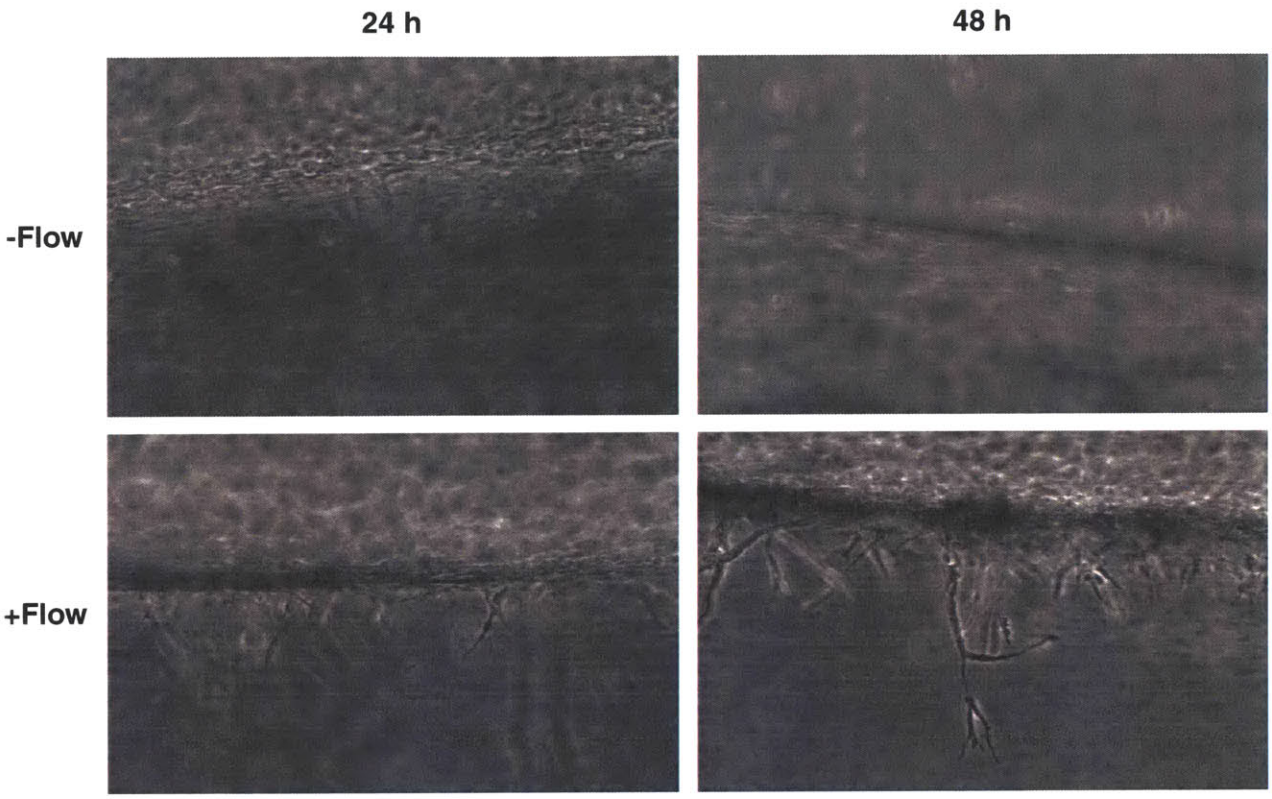

Figure 1: Capillary Morphogenesis with/without Flow
This figure is adapted from Rodrigo's master's thesis

From previous work of Semino et. al. an optimal interstitial flow velocity was around 10μm/min [56], which is much lower than the values used by Swartz et. al. In Rodrigo's study, similar value of optimal interstitial velocity was also observed to be around 10μm/min. This value induced the maximal amount of Src phosphorylation and greatest number of capillary structures was observed.

1.4 Development of Microfluidic Device

The microfludic device is designed and developed by Vernella Vickerman with the assistance from Dr. Sid Cheung. The microfluidic device is highly versatile. It allows for interstitial flow, shear flow, pressure gradient as well as constant chemogradient application. The small scale also allows for better control of the microenvironment. Some baseline results by Vickerman showed that the capillaries were observed in the device (Fig 2). The cells appeared to first migrate as a sheet, but eventually fold up into a tube. Under these conditions, the cells appear to sprout into networks from the beginning.

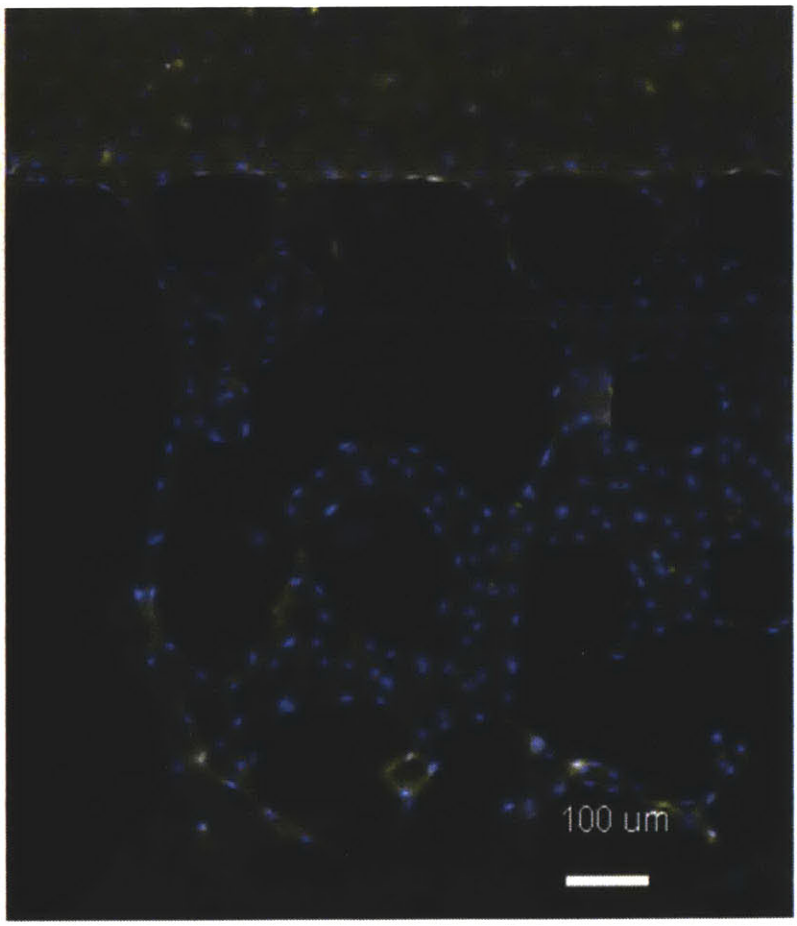

Figure 2: Baseline results from Microfluidic Device
The experiment was performed by Vernella Vickerman under baseline conditions (static and no additional growth factors) and cells were fixed after 7 days of culture

2. Objective

One of the main goals in establishing functional vascularature in tissue engineering is to determine the optimal chemical and physical conditions for the endothelial cells to undergo capillary morphogenesis. The past research has provided ample amount of evidence that fluid flow is essential for angiogenesis both *in vivo* and *in vitro*. Although extensive studies have been conducted, the results are at times contradictory. From the *in vivo* observations, it is suggested that angiogenesis is initiated from nearby venoules or capillaries. This indicates that angiogenesis occurs in a direction opposite to the flow direction. [14] On the other hand, lymphatic cells were shown to migrate along the lymph fluid flow.[49] Simulations also suggested that the flow will create a gradient of chemoattractants in the direction of flow which will encourage cells to undergo chemotaxis.

This project is, therefore, focused on determining the optimal directionality of the fluid flow and to understand how it affects the capillary morphogenesis process. By identifying the differences, we can better utilize the effect of fluid flow in optimizing the physical conditions of capillary morphogenesis *in vitro*.

3. Methods

3.1 Cell Culture

Two types of cells were used: Human Umbilical Vein Endothelial Cells (HUVEC) and Human Adult Microvascular Endothelial Cells (HMVEC) (Cambrex, East Rutherford, NJ). Both cell types were cultured in EBM-2 basal media with respective added aliquots from the manufacturer. (BD Biosciences, MD) Experiments were conducted using cells of passage 6-8. For experiments where vascular endothelial growth factor (VEGF) was used, it is in the form of VEGF-121 prepared following manufacturer's instruction (R&D Systems MN). It is then added to the media.

3.2 Meso-Scale Bioreactor

This device was designed by Rodrigo Hernandez and Carlos Semino. The objective was to design a system in which the invasion of endothelial cells into the collagen gel could be easily observed. In addition, there would be a relative large number of cells so that western blots can be performed.

3.2.1 Device Dimensions

The geometric parameters and the design of the devices are shown in Figure 3 (units in millimeters). The device is made out of Polydimethylsiloxane (PDMS) with a ratio between the base polymer and the curing agent of 8:1 by volume. More details can be found in Rodrigo's thesis. [57]

Basically, the design included two thin halves of PDMS walls which were glued together by silicone adhesive to make the chamber. The walls of the chamber were relatively thin (~ 500μm). This feature enabled better optical resolution. However, the disadvantage of the thinness was the likelihood of bulging out or deforming of the wall.

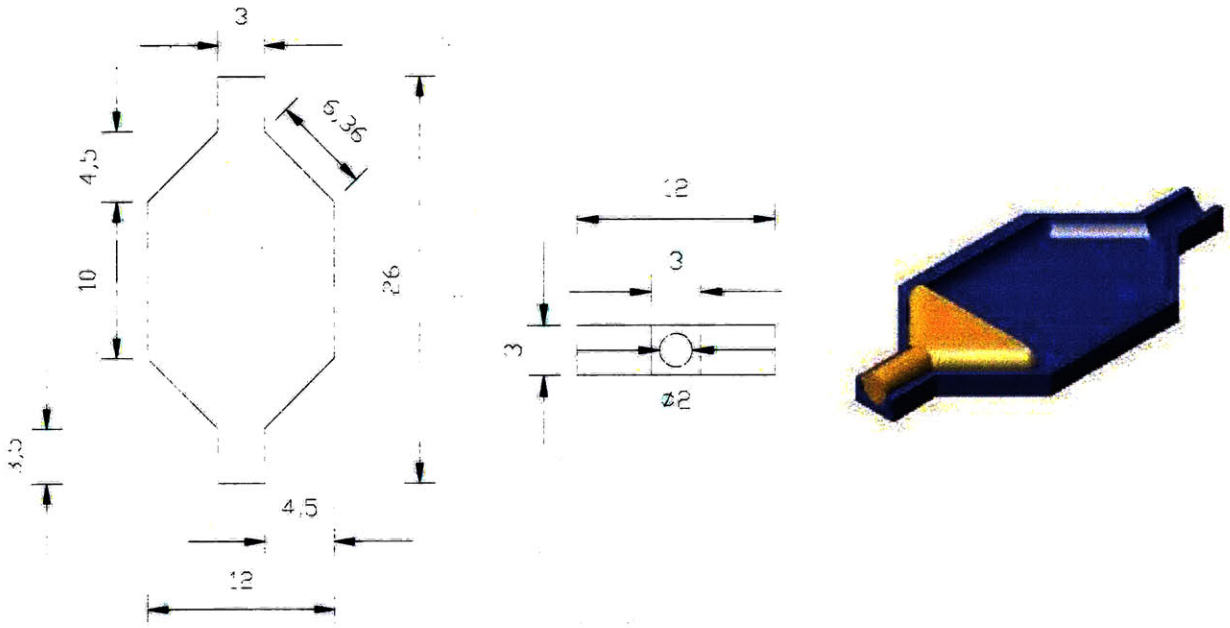

(A) Front View (B) Top View (C) 3D Cross-sectional View

Figure 3: Meso-Scale Bioreactor Design

3.2.2 Gel Loading

Collagen type I from rat tail tendons was used to make the gel scaffold. Solutions with the desired concentration (2mg/ml for most experiments unless noted) were prepared and placed on ice to prevent polymerization. A sterile 21G needle was inserted inside a piece of silicone tubing with inner diameter of 1/32" and outer diameter of 3/32". The purpose of the tubing was to ensure a tight fitting between the bioreactor and the syringe needle. Collagen solution was drawn into the syringe; then the syringe was gently connected to one end of the bioreactor. With the bioreactor in a vertical position, the gel was injected into the bioreactor.

The syringe was slowly withdrawn once the desired amount of collagen was injected (~120 µl). The bioreactor is then placed in a Petri dish in the incubator with 37 °C and 5% CO_2 for 20 minutes allowing polymerization.

3.2.3 Cell Loading

Cells were introduced in three different ways:

1) Cells were mixed inside the collagen solution and the collagen was introduced to the bioreactor as described in the previous section. The cell densities varied from 1-2 x 10^6 cells/ml. Cell suspension solution was centrifuged to form a cell pellet then most of the medium was gently aspirated. Finally, collagen solution was added and mixed vigorously with the cell pellet, and cells were introduced in a three dimensional environment as individual cells. This setup resembles more closely the process of vasculogenesis.

2) Cells were placed on top of the collagen scaffold for monolayer development. After the collagen gel was polymerized, ~100 µl of media was added to the reactor to equilibrate with the collagen gel for 30 minutes. Meanwhile, cell solution was prepared to the desired concentration. 100,000 cells suspended in 100 µl of media were added to the bioreactor and the reactors were placed in a vertical position to allow cells to settle under gravity. Assuming all cells settled on the collagen, the cell seeding density is ~5000 cells/mm^2. Minimal leakage of media was observed since the gel was fully polymerized. Cells were allowed to incubate for 24hrs to develop a monolayer before flow application. This method

models angiogenesis more closely since a monolayer is developed before cells sprout into the surrounding matrix.

3) The third method created a monolayer sandwiched between two layers of acelluar collagen. The procedure was similar to the second method. Once the cells were introduced to the device, they were allowed to settle under gravity and attach to the collagen scaffold for 2 hours. The medium was then gently removed and additional 100μl of collagen was added. Once the second layer of collagen polymerized, fresh medium was added to the device.

3.2.4 Flow Induction

Flow was introduced by a syringe pump. 21G needles were connected to 1ml syringes. 1ml of media was drawn into the syringe. The needle was connected to the same type of tubing as that during gel loading. In addition to ensuring a tight fitting, the tubing also served as the connection between the syringe pump and the bioreactors. The flow diagram can be seen in Fig. 4.

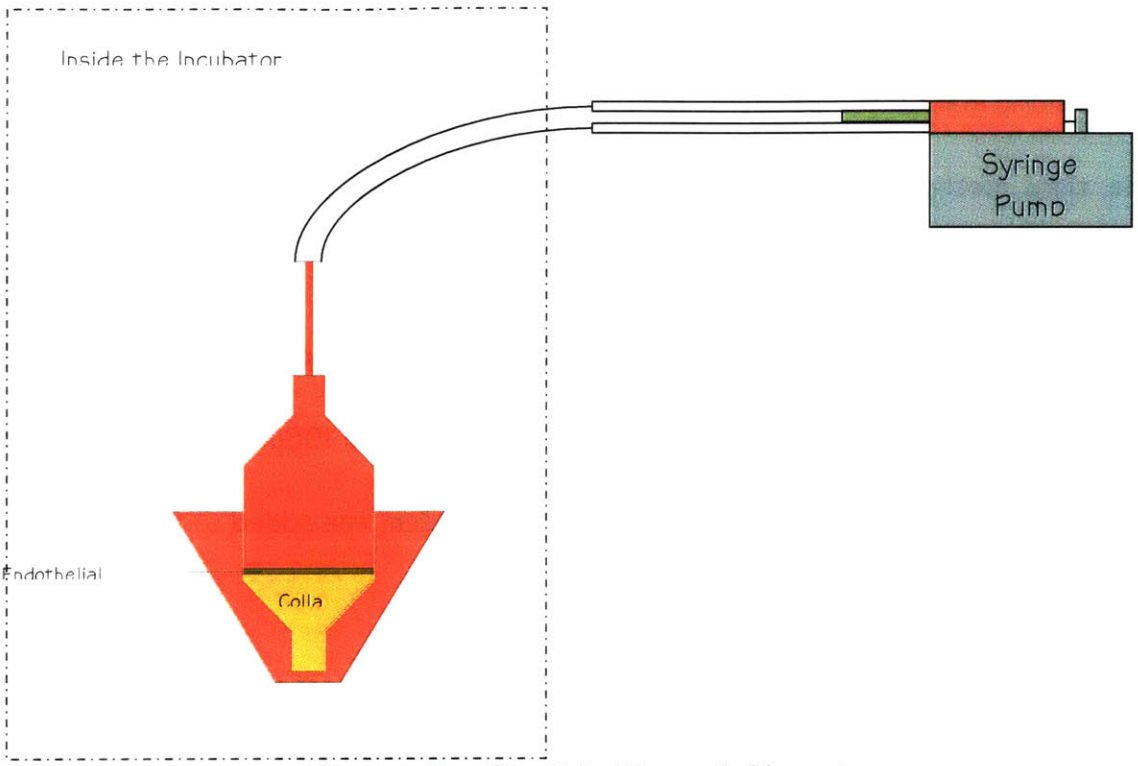

Figure 4: Flow Circuit for Meso-scale Bioreactor

From previous experience, it was found that the optimal interstitial flow velocity for capillary morphogenesis is 10 μm/min. The cross sectional area of the bioreactor is 19.14 mm^2. The flow rate can thus be calculated to be 11.484 μl/hr. This was the flow rate used in all experiments unless specified otherwise.

3.3 Microfluidic Devices

The meso-scale bioreactors were designed to observe the capillary morphogenesis process. However, the thickness of the device made it difficult to observe the details of the angiogenic process. Furthermore, collagen gel sometimes detached from the thin wall of the chamber invalidating the flow experiments. Therefore, another device was used to study similar phenomenon with a better observation capability of the process. Although interstitial

flow was the main focus in this study, the device could also be used to study shear flow and chemical gradients. Thus, it expands the possible applications to this microfluidic device.

3.3.1 Device Dimension

The device was designed by Vernella Vickerman and Dr. Sid Chung in our laboratory. The main objective for this device is to be able to observe capillary morphogenesis over time in a well-controlled physical and chemical environment. The device is consisted of one gel cage region and 2 flow channels. Each channel has two ports which can be connected to media reservoir or pumps. Within the gel cage, there are several PDMS posts as supports for the gel scaffold. The device is made from PDMS. The figure of the device can be seen in Fig. 5 with a zoomed-in picture of the gel cage in Fig. 6.

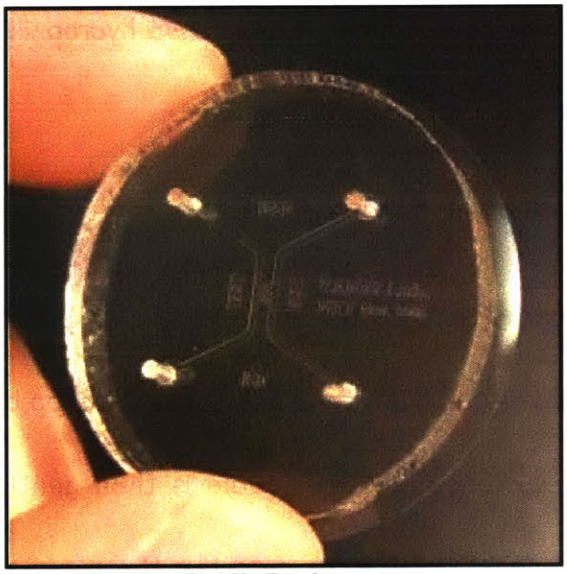

Figure 5: Microfluidic Device

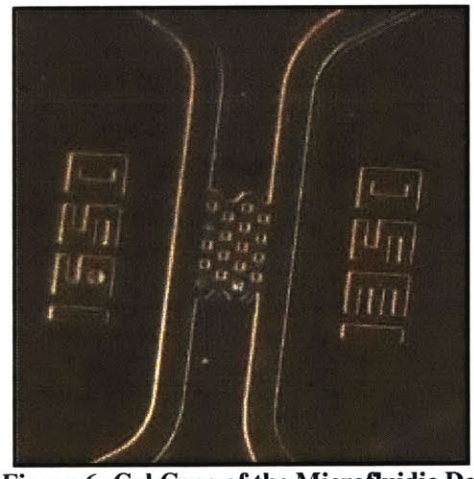

Figure 6: Gel Cage of the Microfluidic Device

The dimensions of the gel cage can be more clearly seen from Figure 8. Each post has the dimension of 100μm x 100μm x 150μm. The width of the gel cage varies from 1350μm to 1650 μm as shown in figure 5. The length of the gel cage is 1020 μm and the height is 150 μm which

flushes by the height of the posts. The staggered arrangement of the posts ensures the security of the gel so that the gel is less likely to flown away.

3.3.2 Device Production and Preparation

The microfluidic device is made out of PDMS in a 10:1 ratio of base elastomer and curing agent by weight. The detailed protocol of the production can be found in Appendix II. Briefly, the mixture is poured on top of a silicon wafer with the negative master. After proper vacuum evacuation and curing, the devices are removed. Punches used for tissue biopsy are used to make the four ports at the two ends of the channels.

Before experiment, the devices are autoclaved on the wet cycle for 20 minutes followed by the dry cycle for 20/10 minutes. The devices are plasma treated 30 minutes before gel loading. The purpose of plasma treatment is to make the surface of the PDMS hydrophilic enough so that when gel is loaded, it will evenly distribute through the gel cage.

3.3.3 Gel Loading

The collagen gel preparation procedure is the same as that for the meso-scale bioreactor. Once the gel solution is prepared, it is microinjected into the device. When loading, a drop of collagen solution is suspended at the tip of the microneedle. The needle is then gently moved down so that the collagen touches the gel cage and speads onto the the plasma-treated PDMS surface. Roughly 1 μL of collagen solution was injected. The injection process was monitored through a real-time microscope (Digital Blue QX3). Some collagen solution would leak out into the channels but no blockage of the channels was observed. Once the

solution was placed into the gel cage, a #1 coverslip was placed on top. The hydrophilicity is strong enough to create a tight seal between the PDMS device and the coverslip. The assembled device is then placed in a humidified box and placed in the incubator for 30-45 minutes for proper polymerization.

3.3.4 Cell Loading

Cells were seeded as a monolayer. Once the gel was polymerized, media was slowly introduced into both channels. Cell solution (10^6 cells/ml) was prepared as described in Appendix II. 60μL of the cell solution was placed on one port and it was slowly withdrawn with a 20 μL pipette on the other side of the channel. A much smaller drop of cell solution (~10 μL) was then placed on the second port where the pipette had been. The different curvature of the cell solution bubble acted as a passive pump which encouraged the constant flow of cell solution. The devices are placed vertically to allow cells to settle under gravity for 30 minutes.

The devices were examined under the microscope to ensure proper cell attachment. One drop of media was placed on top of each port to prevent dehydration of the gel and allow nutrient diffusion. If flow was to be introduced, it was applied after 24hour static incubation to allow proper monolayer development. Figure 7 is a schematic drawing of the final setup.

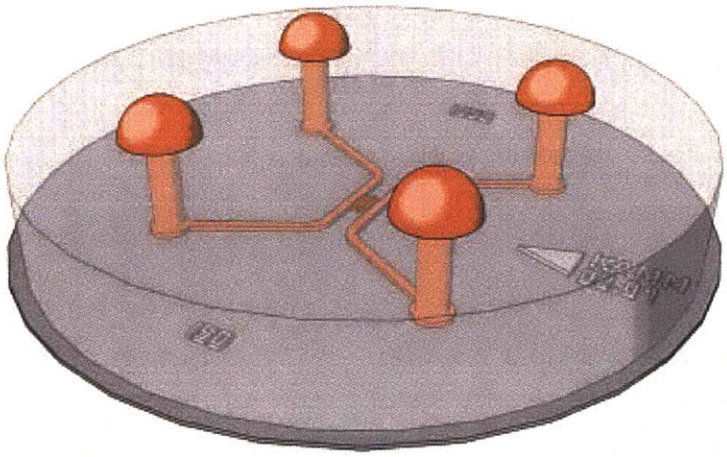

Figure 7: Schematic Drawing of the final setup of the Microfluidic Device

3.3.5 Flow Induction

Hydrostatic pressure differential, modulated by surface tension effects, was used to produce flow. Each port was connected to a 200 µL pipet tip. By placing more media in the two tips on one side compared to the other side, a pressure drop was developed across the gel. The pressure drop was monitored through the duration of the experiment. Every 24 hours, the change in height was noted and half of the media was closely aspirated out from each pipet tip. Fresh media was then added to maintain the pressure difference.

3.4 Flow Velocity and Permeability Calculations

Since the flow was maintained with the hydrostatic pressure difference, it will vary through the duration of the experiment. By measuring the volume of media that flows across the gel in a given length of time, an average flow rate can be calculated. This calculation assumes that the entire volume of medium flows through the gel and that the effect of evaporation in the incubator was negligible. Computed in this way, the flow rate is roughly 1µL/hr with the initial pressure drop of 50Pa.

Because of the staggered arrangement of the posts, the cross sectional area of the gel varies. An effective cross sectional area is then calculated. Figure 8 provides a closer view of the gel cage. Equation 1 calculates the effect cross sectional area of the gel cage. As mentioned earlier, each post is 100μm wide and the space between each post is 150μm.

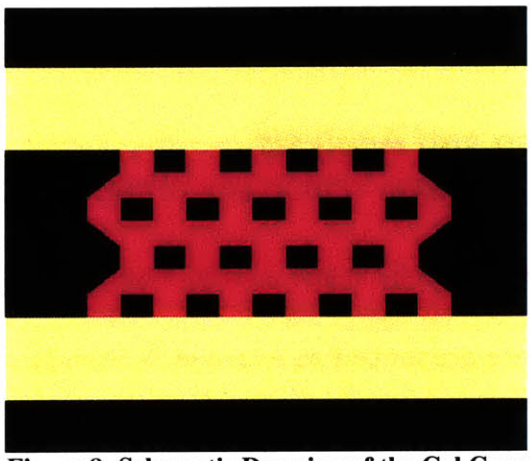

Figure 8: Schematic Drawing of the Gel Cage
(Not drawn to scale)

$$\left[\frac{2}{7}(5\cdot 150\text{um}) + \frac{2}{7}\cdot(6\cdot 150\text{um}) + \frac{3}{7}\cdot(5\cdot 150\text{um} + 5\cdot 100\text{um})\right]\cdot 150\text{um} = 1.511\times 10^{5}\ \text{um}^{2}$$

Equation 1: Effective Cross-sectional Area

The flow velocity can therefore be calculated to be

$$\text{FlowVelocity} = 120.662\frac{\text{um}}{\text{min}}$$

Equation 2: Flow Velocity of the Microfluidic Device

With a first order calculation assuming the pressure drop is constant over 24 hours, the permeability can be calculated by using Darcy's Law (Equation 2 & 3).

$$V = k\cdot\frac{\Delta P}{L}$$

Equation 3: Darcy's Law

$$K(h) := \frac{\text{FlowRate}\cdot\text{WidthCage}\cdot\mu}{\text{CSA}\cdot P(h)}$$

Equation 4: Rearranged Form of Darcy's Law to Calculate Permeability

$$K(5mm) = 4.1 \times 10^{-10} cm^2$$

Equation 5: Hydraulic Conductivity of the 2mg/ml Collagen Gel in the Microfluidic Device

From this first order magnitude, we obtained the permeability to be on the order of 10^{-10} cm^2 which is smaller than some reported values, $10^{-8}cm^2$ for 2.5mg/ml collagen from Wang and Tarbell and $1.2x10^{-8}$ cm^2 for 1mg/ml collagen + 1mg/ml fibrinogen [58, 59]

3.5 Image Acquisition and Analysis

Images were acquired with the Nikon TEH100 with OPENLAB 4.0.4 software. Measurements of length, area or angle were done by Image J (NIH). Analyses were performed with Microsoft Excel. Unless noted, data are presented as Average ± Standard Deviation.

4. Results

4.1 Meso-scale Bioreactors

The experiments done with the meso-scale bioreactors were categorized based on how the endothelial cells were seeded and their relations with the collagen scaffolding. Three types of arrangements were made as mentioned in the earlier sections. Cells were seeded as a monolayer on top of the collagen scaffold or in between two collagen scaffolds. Sprouting from a well-developed endothelial cell monolayer was used as a model for angiogenesis. Another way cells were seeded was suspension inside the collagen scaffold. This method mimics more closely to the three dimensional environment endothelial cells experience during vasculogenesis. Figure 9 illustrated the three different experimental setups.

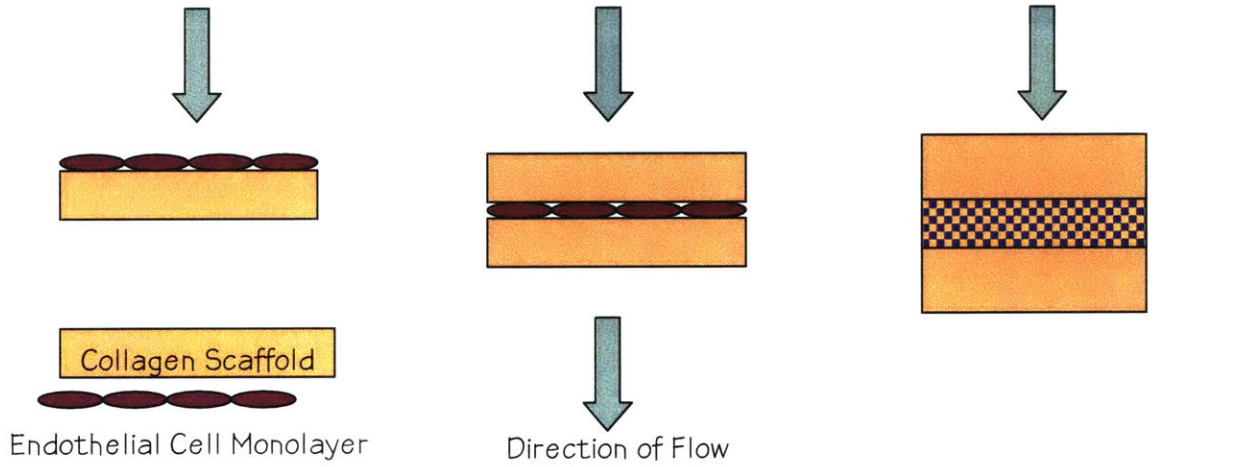

(A) Monolayer on Top of Collagen Scaffold

(B) Monolayer Sandwiched between Two Layers of Collagen

(C) Cells suspended inside Collagen Gel Scaffold

Figure 9: Schematics of Three Different Experimental Setups

4.1.1 Capillary Morphogenesis from Endothelial Cell Monolayer

In this section, the results refer to the experimental setup (A) in Figure 9. Capillary morphogenesis from endothelial cell monolayer has been studied extensively by Rodrigo. Some of the key findings were described in the background section. From running experiments of the same setup, I was able to reproduce the results from his work. Sprouts were observed under a low flow velocity (10 μ m/min as determined before) for 24 and 48 hours (Figure 10).

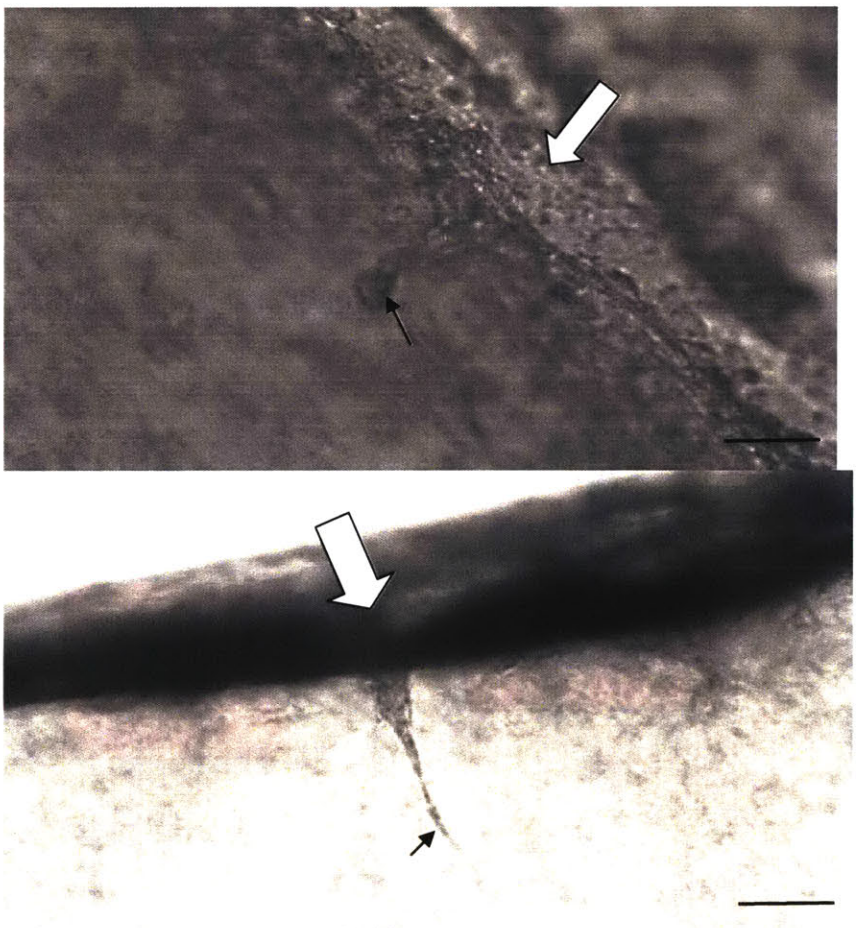

(A) Sprouting from Monolayer after 24 hours

(B) Sprouting from Monolayer after 48 hours

Figure 10: Sprouting from Monolayer at Two Different Time Points
Arrows indicate sprouts while the block arrow is the direction of flow. Flow velocity was 10μm/min. Scale Bar: 50 μm

4.1.2 Capillary Morphogenesis from Endothelial Cell Monolayer Sandwiched between Collagen Scaffolds

From the previous section, it was shown that sprouting occurred when seeded as a monolayer. To test whether the direction of flow influences the direction of sprouting, Cells were seeded on top of collagen gel as described in the Materials and Method's section. Cells were left to settle and attach on the collagen for 30-45 minutes. The medium was then gently aspirated out of the meso-scale reactor. A second layer of collagen was then added to create an endothelial cell monolayer sandwiched between two layers of collagen. In this setup, I was able to determine whether there was a preferential directional sprouting.

Within twenty four hours of initial setup, the monolayer reorganized into 2D ring-shaped structures (Figure 11). Simliar results have been reported earlier by Montesano et. al.. [60] This structure was stable through the duration of the experiment and appeared to be insensitive to the experimental parameters such as growth factors or flow velocity.

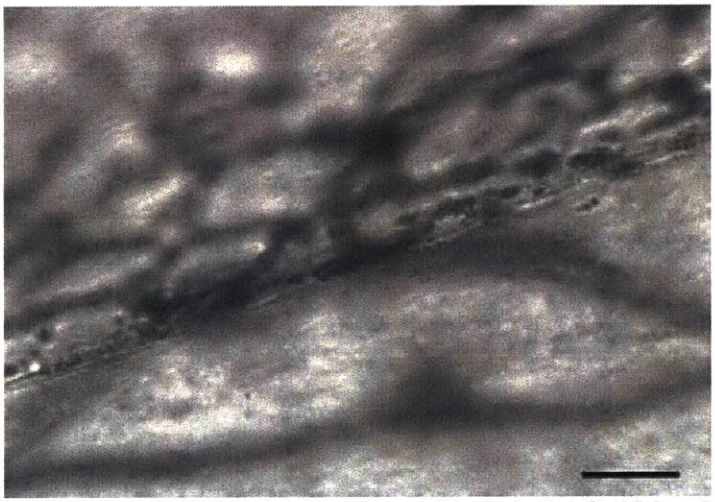

Figure 11: Ring-shaped Reorganization of Endothelial Cell Monolayer
Scale Bar: 50μm

At static or low velocity (10 μm/min), the monolayer reorganized, but no sprouting was observed. Sprouting was only observed when the flow velocity was higher than 50 μm/min. The

length and branching of the capillary-like structures were similar to those not sandwiched between collagen gel layers. Figure 12 demonstrates the sprouts under flow.

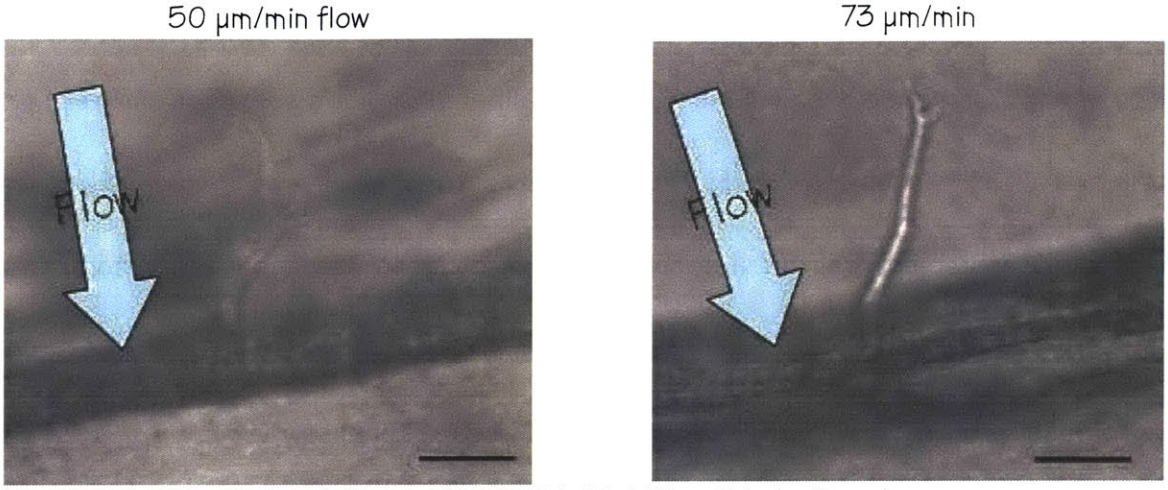

Figure 12: Sprouts Observed in High Flow Velocity Experiments
Scale Bar: 50μm

Many capillary-like structures were observed to invade in the direction opposite from the direction of flow. Length of the sprouts and the angle between the sprout and the direction of flow were measured (Figure 13 and 14).

From Figure 13, there were several key observations. First, the average length of the capillary-like structures was longer for the upstream sprouts than those for the downstream. After 48 hours of flow, only one single sprout was observed in four samples for the downstream flow condition (the purple check-marked bar). As a result, no standard deviation was available. Similarly, by 72 hours of flow, no sprouts could be found in the downstream direction. For the measurements for the angle, it appeared that as the experiment progressed, the upstream sprouts started to align with the flow with decreasing measured angle. The same alignment trend was not observed in the sprouts downstream from the flow.

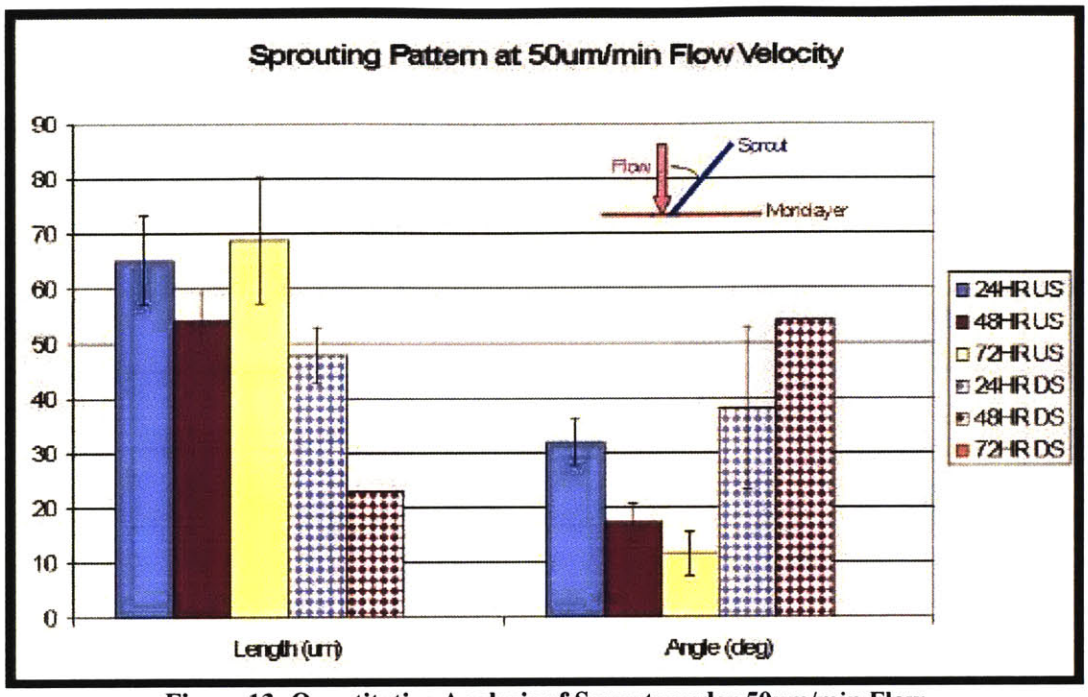

Figure 13: Quantitative Analysis of Sprouts under 50µm/min Flow

At an even higher flow velocity (Fig. 14), fewer capillaries were observed, especially in the downstream direction. Therefore, no data were available for the downstream sprouts. For the upstream sprouts, the length of the sprout reached maximum at around 48 hours of flow. This was not observed at the 50µm/min flow experiment. The length of the sprouts was significantly shorter at 72 hours than the other two time points. The sprout alignment with flow was not observed for the higher flow experiment.

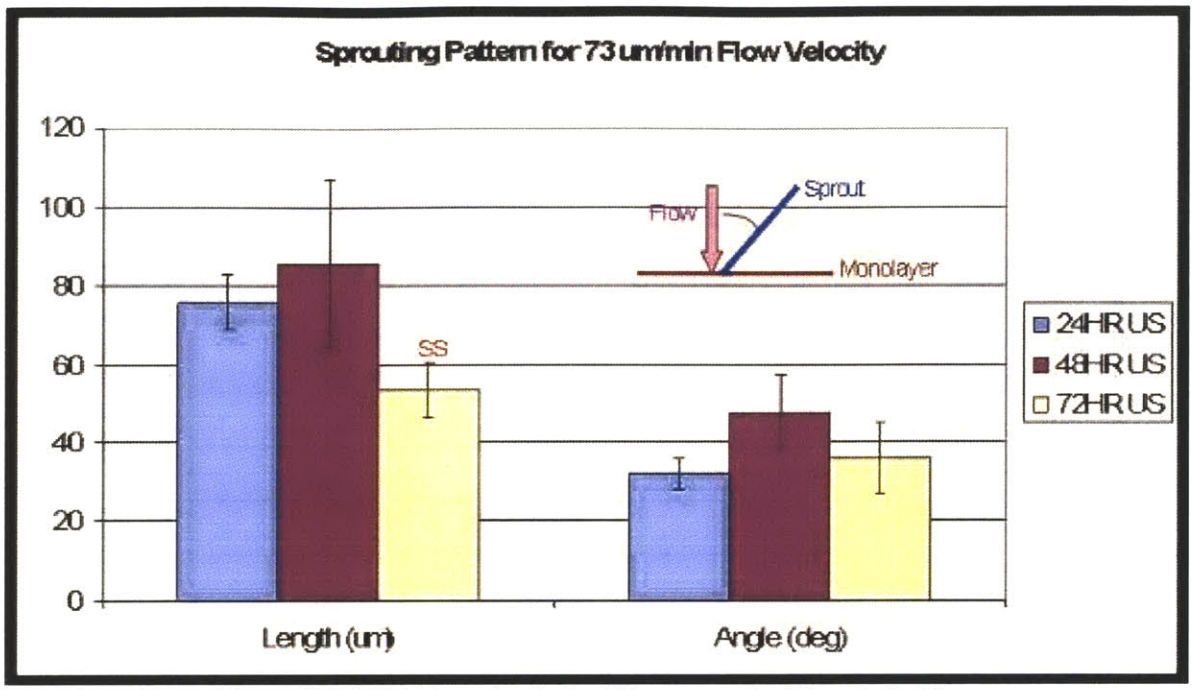

Figure 14: Quantitiave Analysis of Sprouts under 73 µm/min Flow

4.1.3 Capillary Morphogenesis from Suspended Cells in Collagen

The third way to introduce cells in the flow system was to suspend them in the collagen gel solution before polymerization. Cells, in this case, are in a three dimensional space and the cell-cell contact is different from an endothelial monolayer. In this particular experimental setup, three collagen layers were placed in each bioreactor. The layer with cell suspension was sandwiched between two acellular layers. Two distinct phenomena were observed: the connections within the cellular layer and cell migration into the acellular layers.

First of all, a static experiment was run to determine the optimal conditions for cell survival, network formation, cell types and serum level (Figure 15). Complex network within the cell-suspended collagen layer was observed when the cell density was higher than 1.5×10^6/ml. The optimal density appeared to be at 2×10^6/ml. At 1×10^6 cells/ml, little network formation was

observed. HUVECs were more likely to form networks regardless of the serum level. The higher the cell density, the better the network formation appeared to be. Without flow, HUVECs appeared to survive better than HMVECs. Furthermore, the behaviors of HUVECs and HMVECs were distinctly different. While HUVECs were more likely to extend out to form networks, HMVECs seemed to aggregate and form spheroids and clusters. Higher serum level helped HMVECs survival, but not network formation.

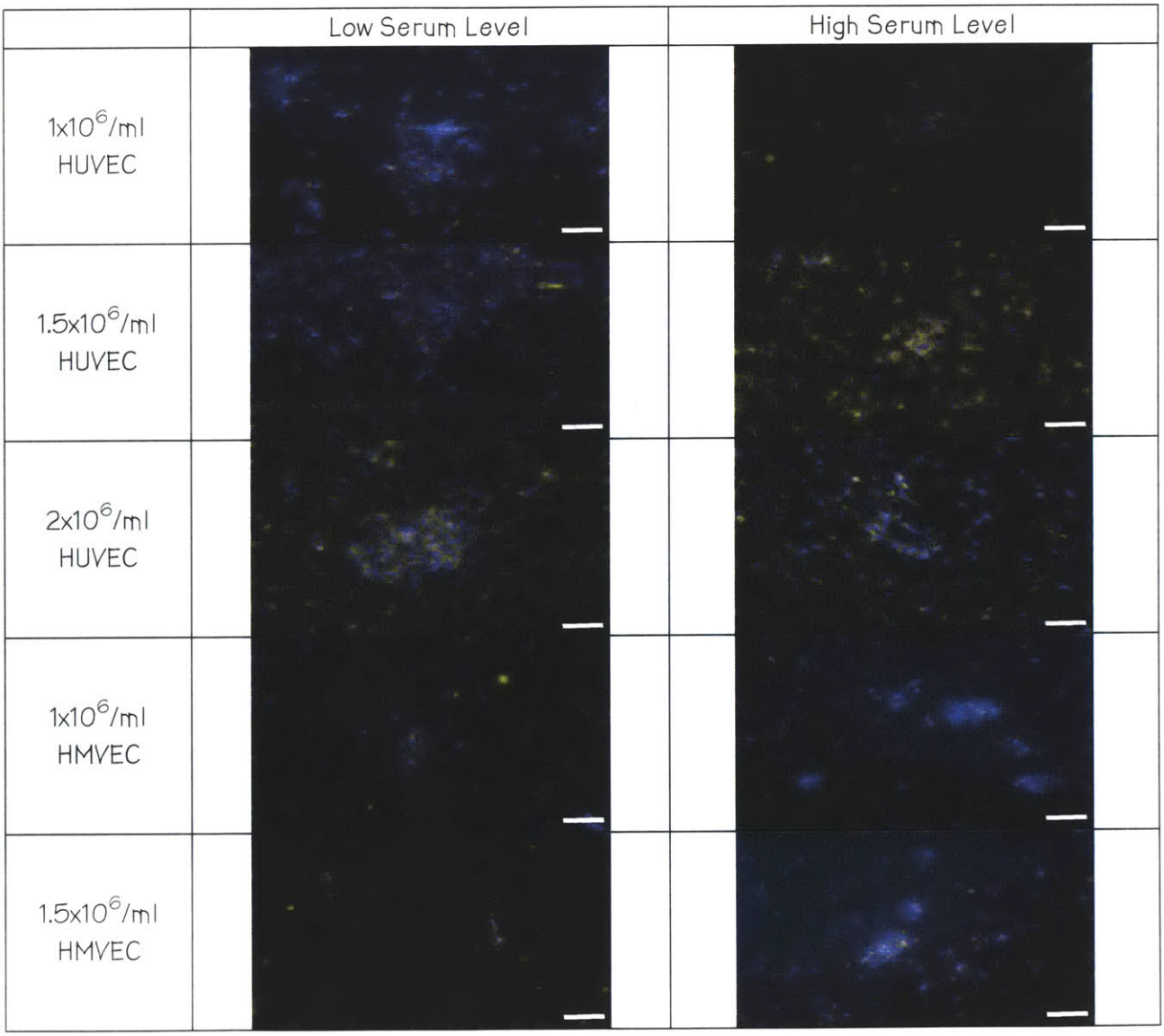

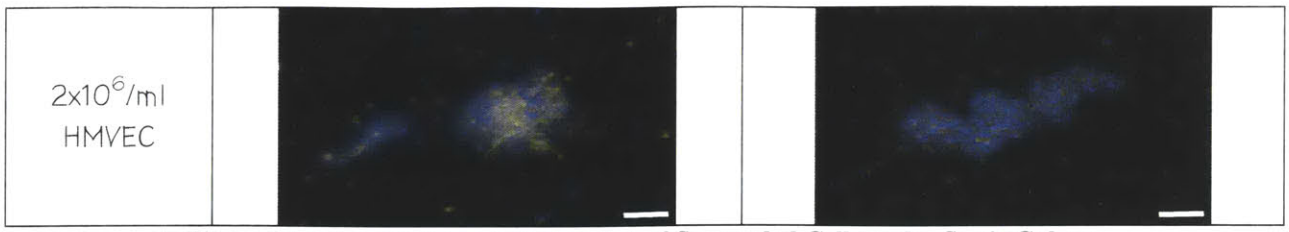

Figure 15: Internal Network Formation of Suspended Cells under Static Culture
Low serum level is the baseline serum provided with the EBM-2 media which is 2% for HUVECs and 5% for HMVEC. For additional serum, FBS was added to 10% for HUVECs and 12.5% for HMVECs. Scale bar: 100μm

In addition to serum levels and cell seeding density, the presence of growth factor, VEGF, and flow (50μm/min) were also studied to understand their effects on internal cell network formation. The presence of VEGF and flow both enhanced the network connections and survival of HUVECs (Fig. 16 and 17)

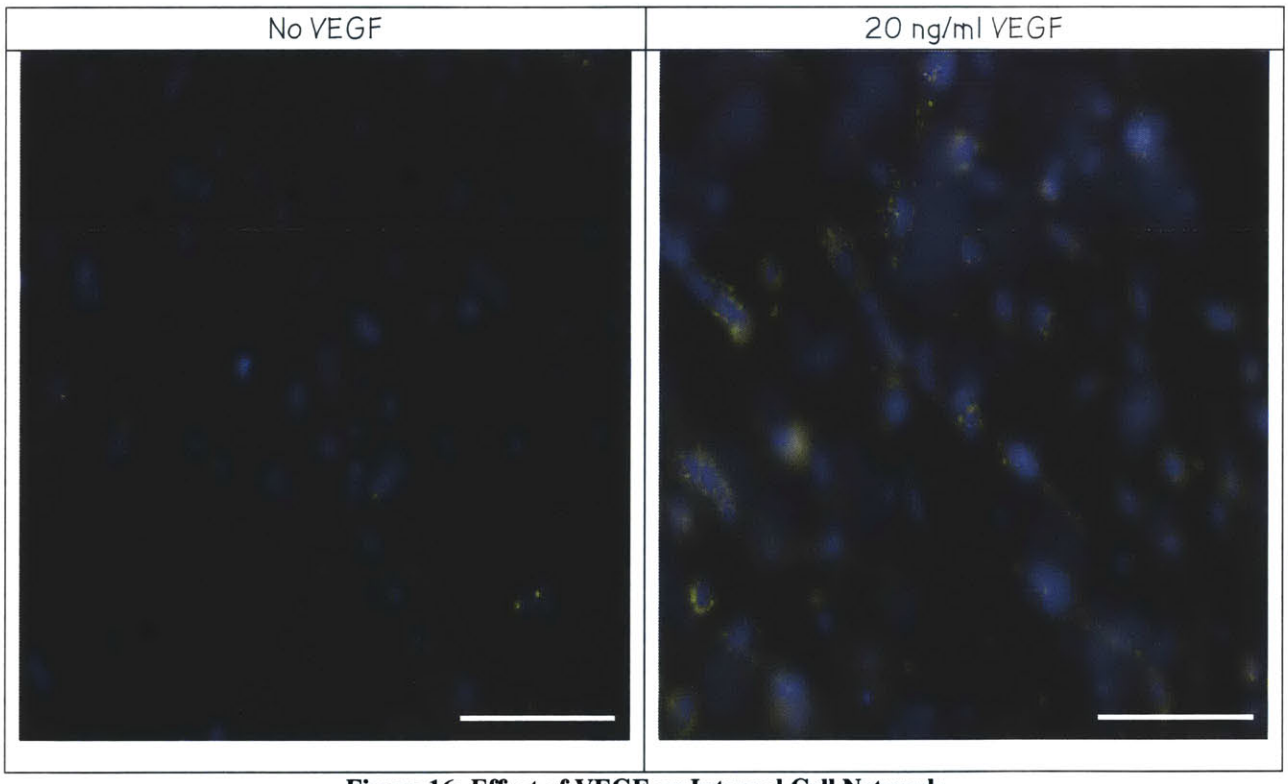

Figure 16: Effect of VEGF on Internal Cell Network
This is an image picture after 48hr of flow (50μm/min).
Scale bar: 50μm

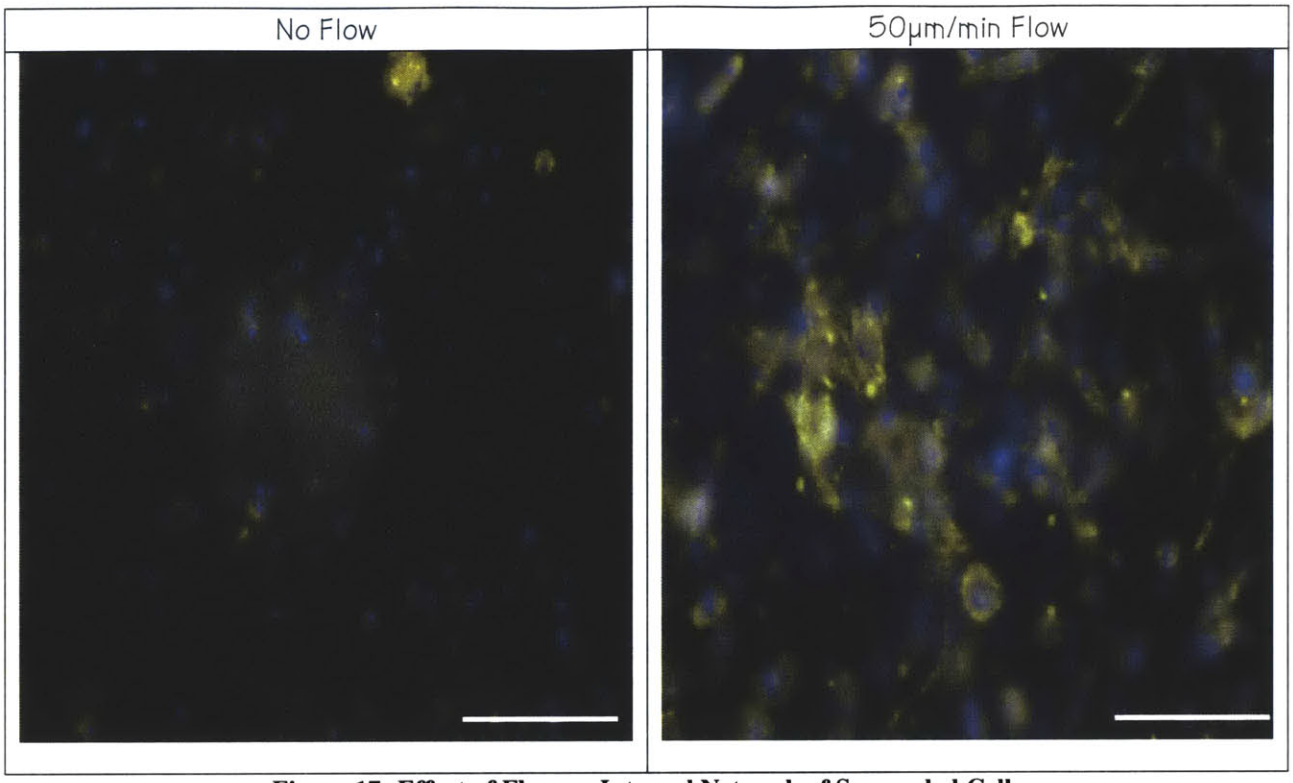

Figure 17: Effect of Flow on Internal Network of Suspended Cells
Scale bar: 50μm

Another key experimental observation was the extent of cell migration into the accellular regions and the goal was to determine whether a preferential direction of migration based on the flow existed or not. Similarly to the monolayer sandwiched between two layers of acellular collagen gel, more cells migrated toward the top, despite the downward flow direction. Out of the 18 samples tested, only 1 invaded into the bottom aceullar layer of collagen. Figure 18 shows 3 representative pictures. The flow direction was from top to down at 50μm/min.

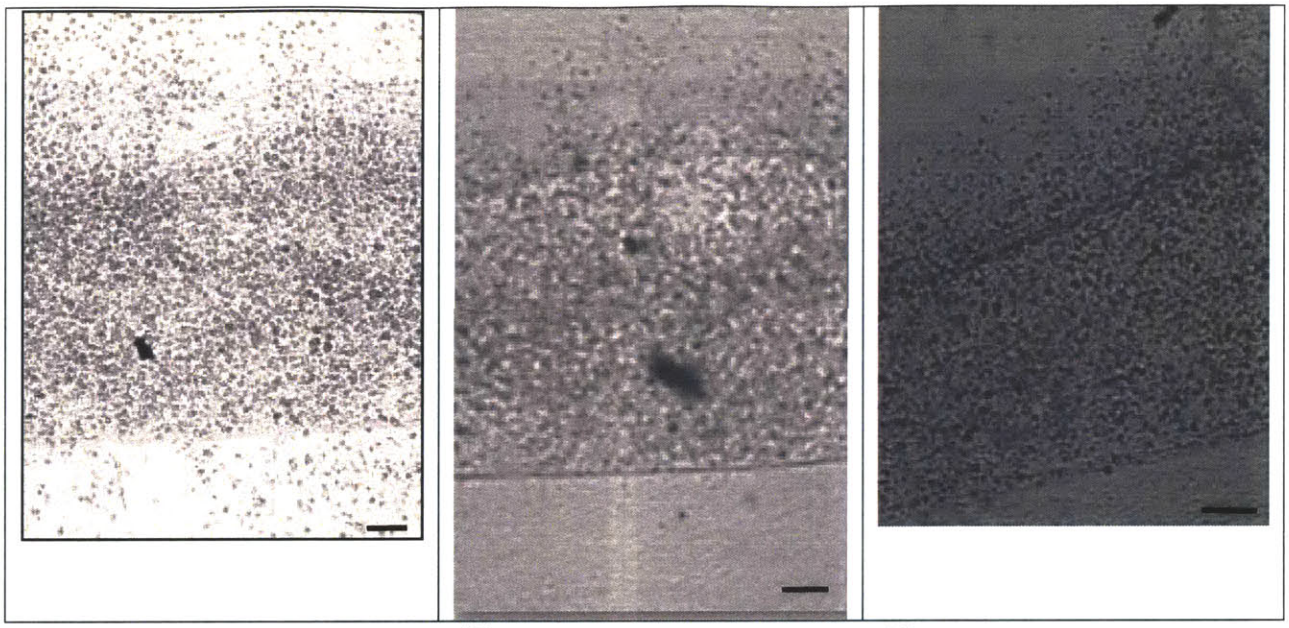

(A) (B) (C)

Figure 18: Invasion into the Acelluar Collagen Layers
Scale bar: 400μm. Figure 16.A was the only sample out of 18 tested which showed migration into the bottom acellular layer of collagen gel. Figure 16.B and C were taken at 24 and 48 hours of flow respectively. Clear separation between the bottom acellular region and the cell-suspended layer was observed in both cases.

4.2 Microfluidic Device

The biggest advantage of the novel microfluidic device allows for the application of interstitial flow with better imaging resolution and better controlled microenvironment because of the small scale. In these devices, collagen gel was microinjected into the gel cage. After gel was polymerized, cells were introduced to one flow channel and allowed to settle on one side of the collagen gel. By applying different pressure head across the gel cage, an interstitial flow could be established. Images were taken daily and experiments lasted for as long as 10 days with high cell viability.

4.2.1 Capillary Morphogenesis from Endothelial Cell Monolayer

Some sprouts were observed similar to the ones in the meso-scale devices (Figure 19). For most experiments, the sprouting phenomenon was, however, overwhelmed by cell migration. As it was later discovered, the collagen gel contracted extensively and the cells were migrating in 2D along the collagen gel surface. Nevertheless, in the sprouts, concentrated DAPI stain, a sign of cell division, is observed near the tip in sample (A). Mitotic behavior near the tip of the sprout is consistent to previously reported results. [14]

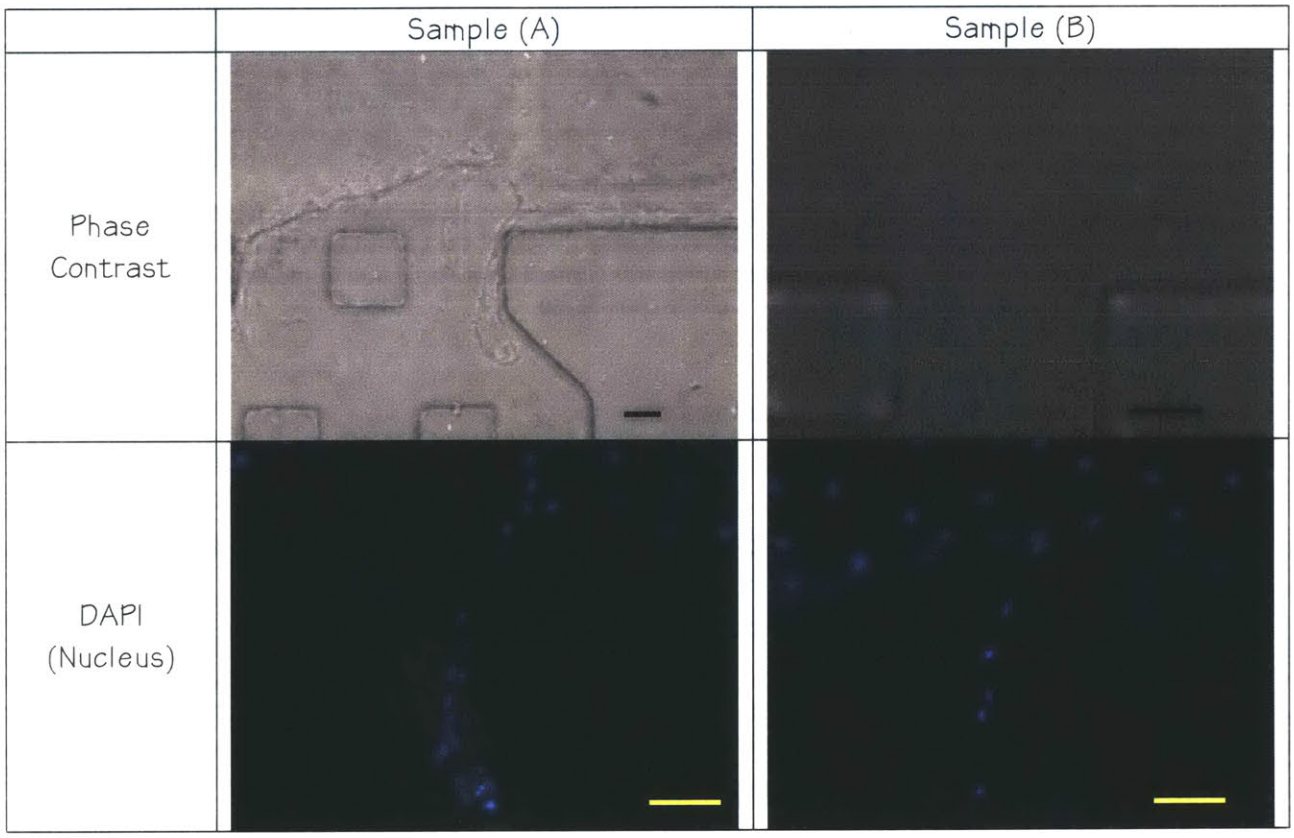

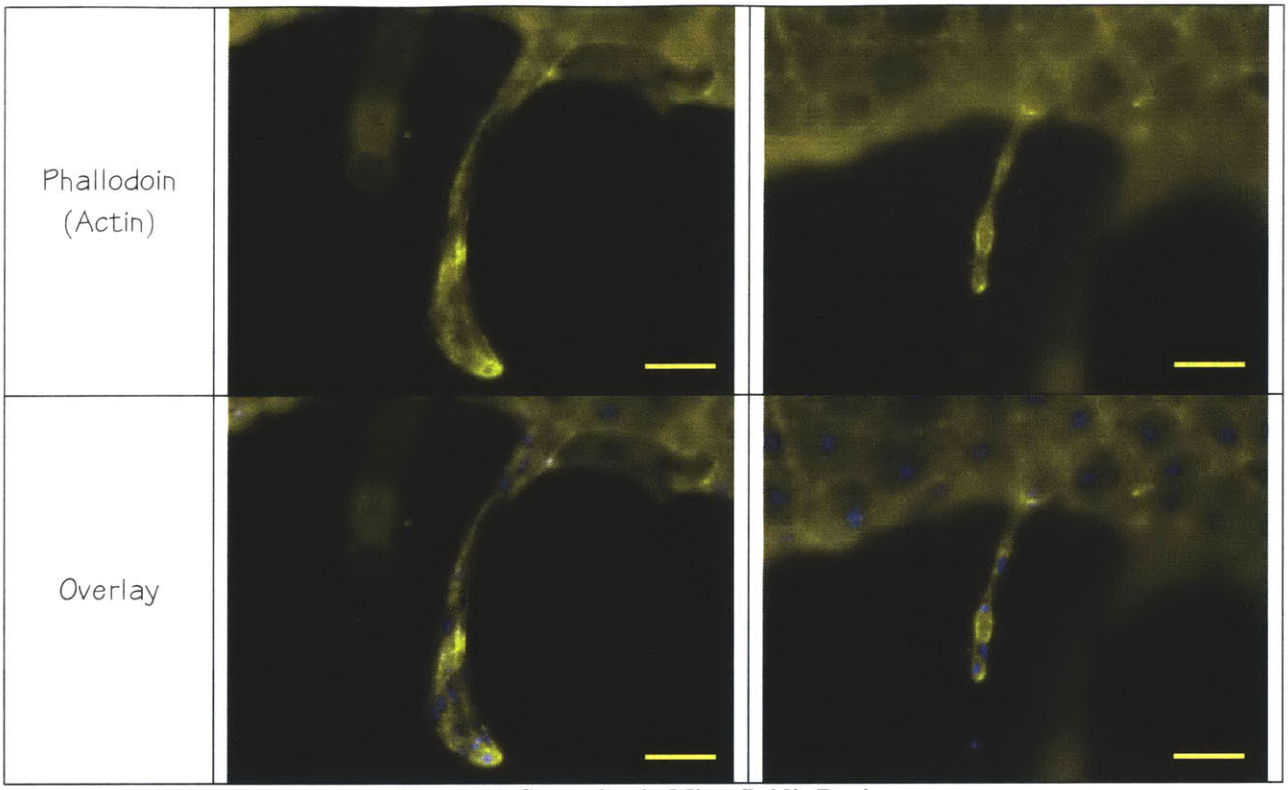

Figure 19: Sprouting in Microfluidic Device
Sample (A) appeared to have multiple cells which suggested lumen formation. Furthermore, it is interesting to notice the mitotic behavior near the tip of the sprout from the DAPI stain. Sample (B) is an adjacent sprout which was formed by a single line of multiple cells. Scale Bar: 50μm

4.2.2 Extent of Cell Migration

As mentioned previously, the extent of cell migration overwhelmed the process of sprouting. Many cells migrated across the entire gel cage through the duration of the experiment (Figure 20) and migration appeared to have no correlation with the direction or existence of fluid flow in this particular experimental setup. Migration also seemed to be equally effective for both HUVEC and HMVEC. Although observations seemed to suggest HUVECs being more active and migrated further, it did not turn out to be statistically significant.

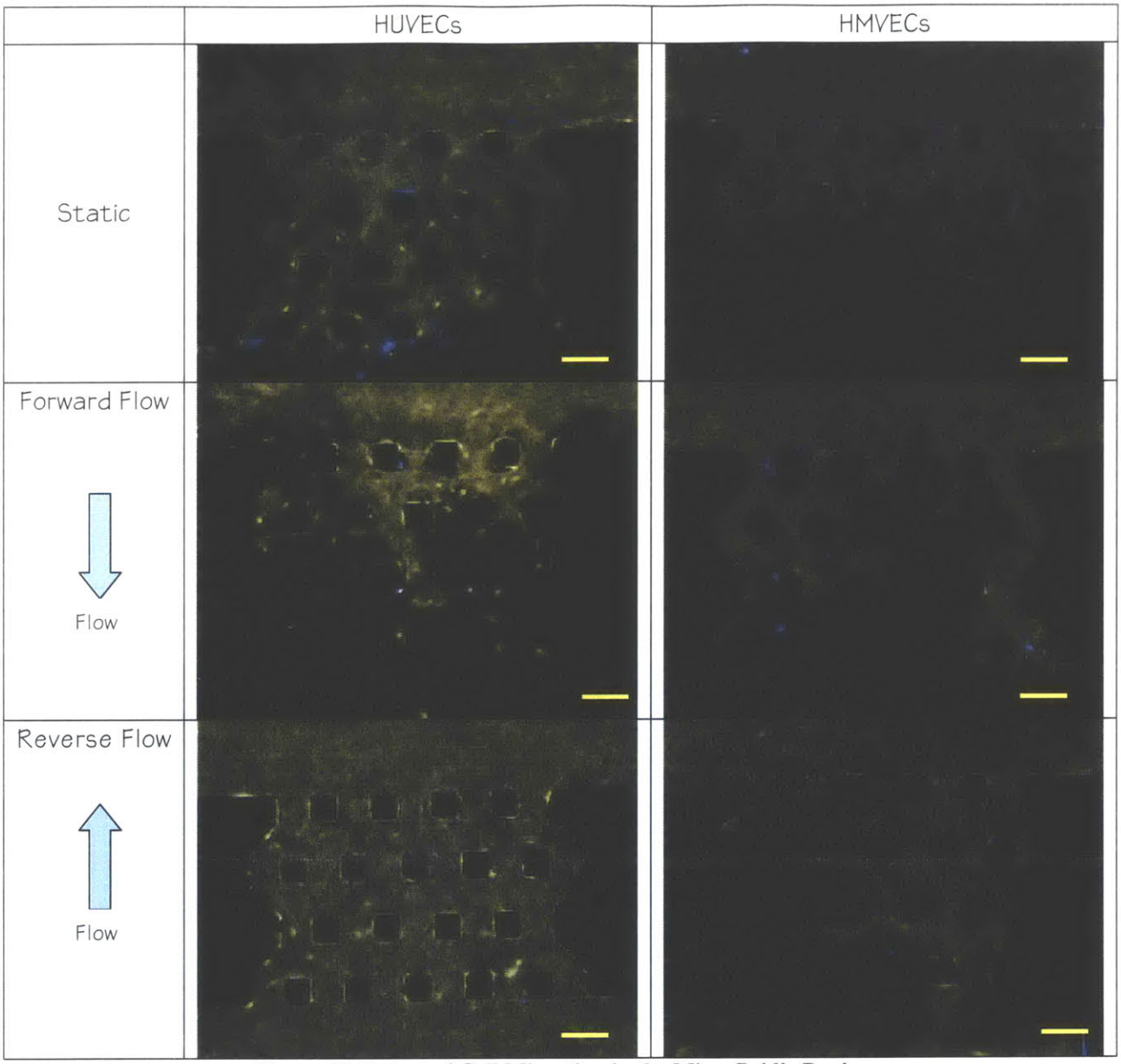

Figure 20: Extent of Cell Migration in the Microfluidic Device
Scale Bar: 200μm

4.2.3 Formation of Multiple Monolayers

As cells migrated into the gel cage and began to contract the gel, small gap spaces were created between the PDMS/coverslip and the collagen gel. Endothelial cells formed monolayers on the collagen gel, so at least two monolayers were observed. (Figure 21) By comparing sample (B) and (D) with (A) and (C), it can be seen that HUVECs appeared to form

more network-like structures and cells were more elongated. For each monolayer, HMVECs tend to spread out in a round shape.

With the exception of the figure near the coverslip for sample (D), none of the other cell migration occurs at the post locations. This indicated that the monolayer was formed on the gel where cells had to go around the post to migrate forward. Gel contraction due to cell migration was readily observed. The collagen scaffold contracted around the posts, most obviously observed in the "intermediate" region of the gel.

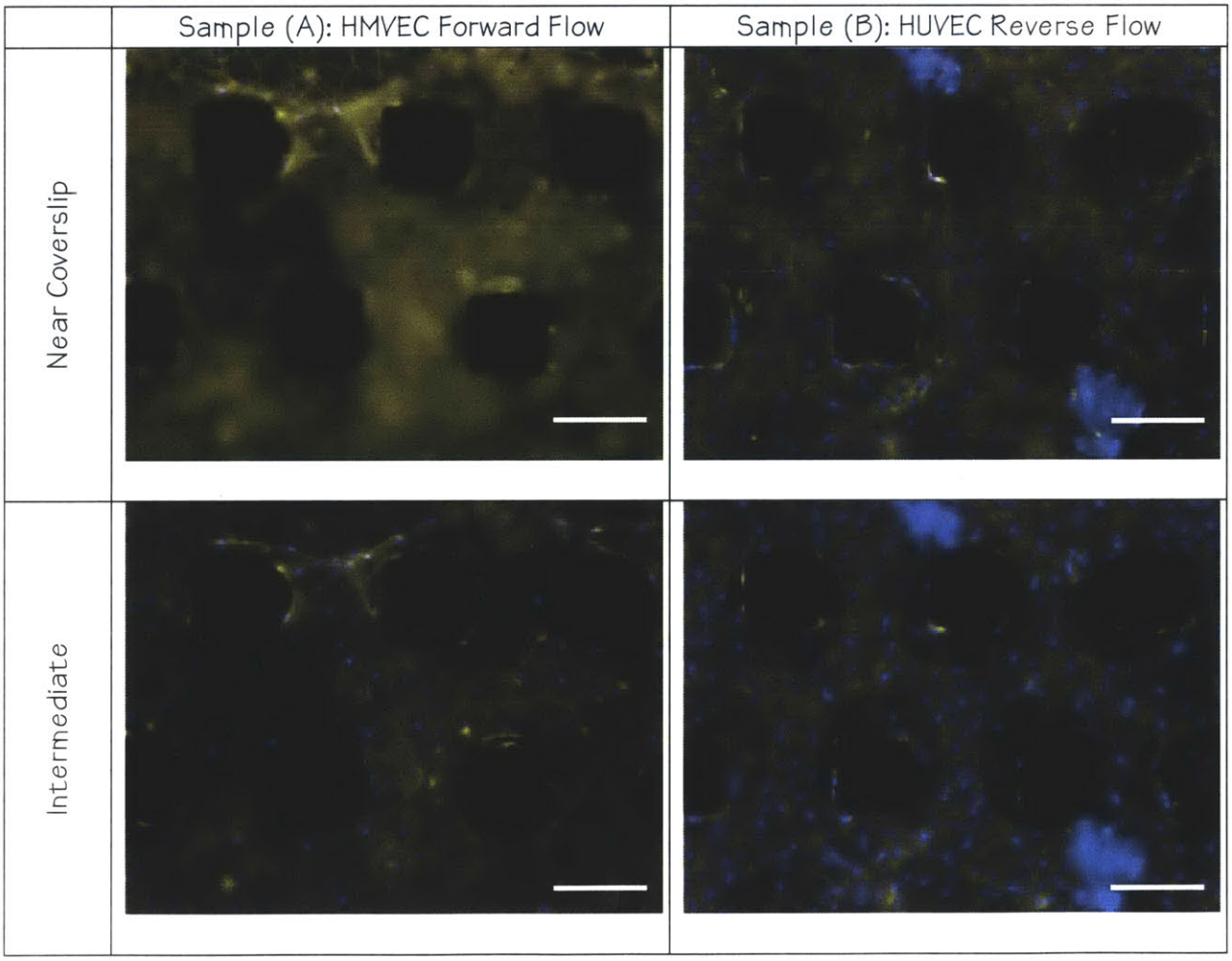

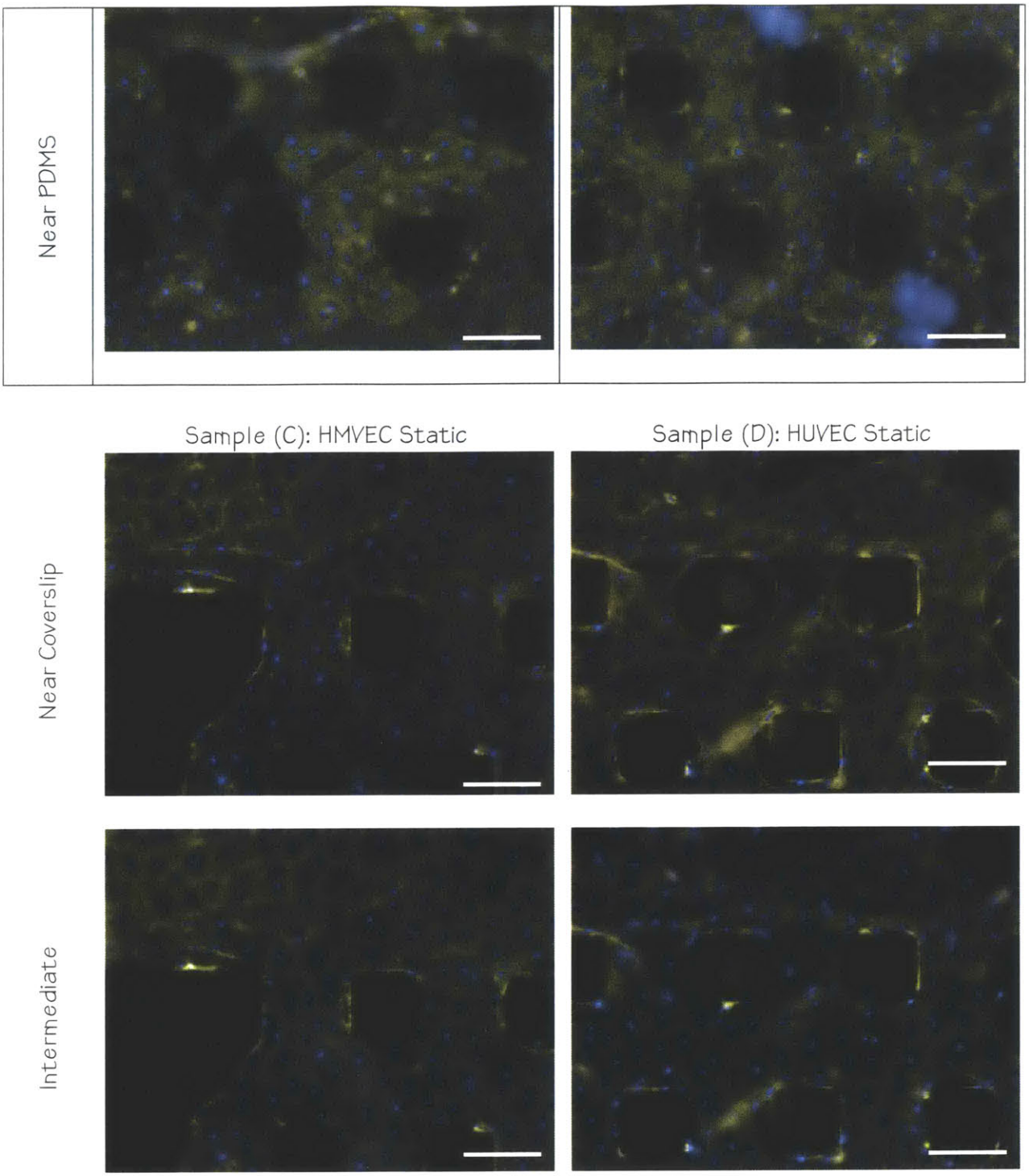
Near PDMS
Sample (C): HMVEC Static
Sample (D): HUVEC Static
Near Coverslip
Intermediate

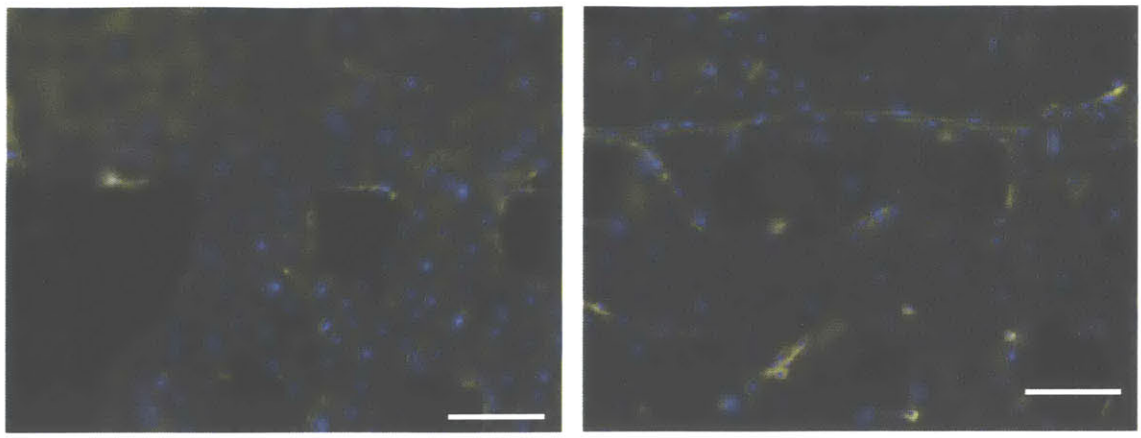

Figure 21: Fluorescent Images of the Endothelial Cell Migration: Formation of Multiple Monolayers
Scale bar: 100μm

4.2.4 Formation of Connections between Monolayers

From a detailed observation of the 2D images, connections formed by actin could be found between the upper and lower monolayers (Figure 22). To look into this possibility more in depth, a microscope equipped with a piezo-stage which allows fine control of the height of the image plane was used to obtain images every 1μm. After the images were taken, they were deconvoluted to reduce noise, and finally stacked to visualize possible three-dimensional structures. (Figure 23).

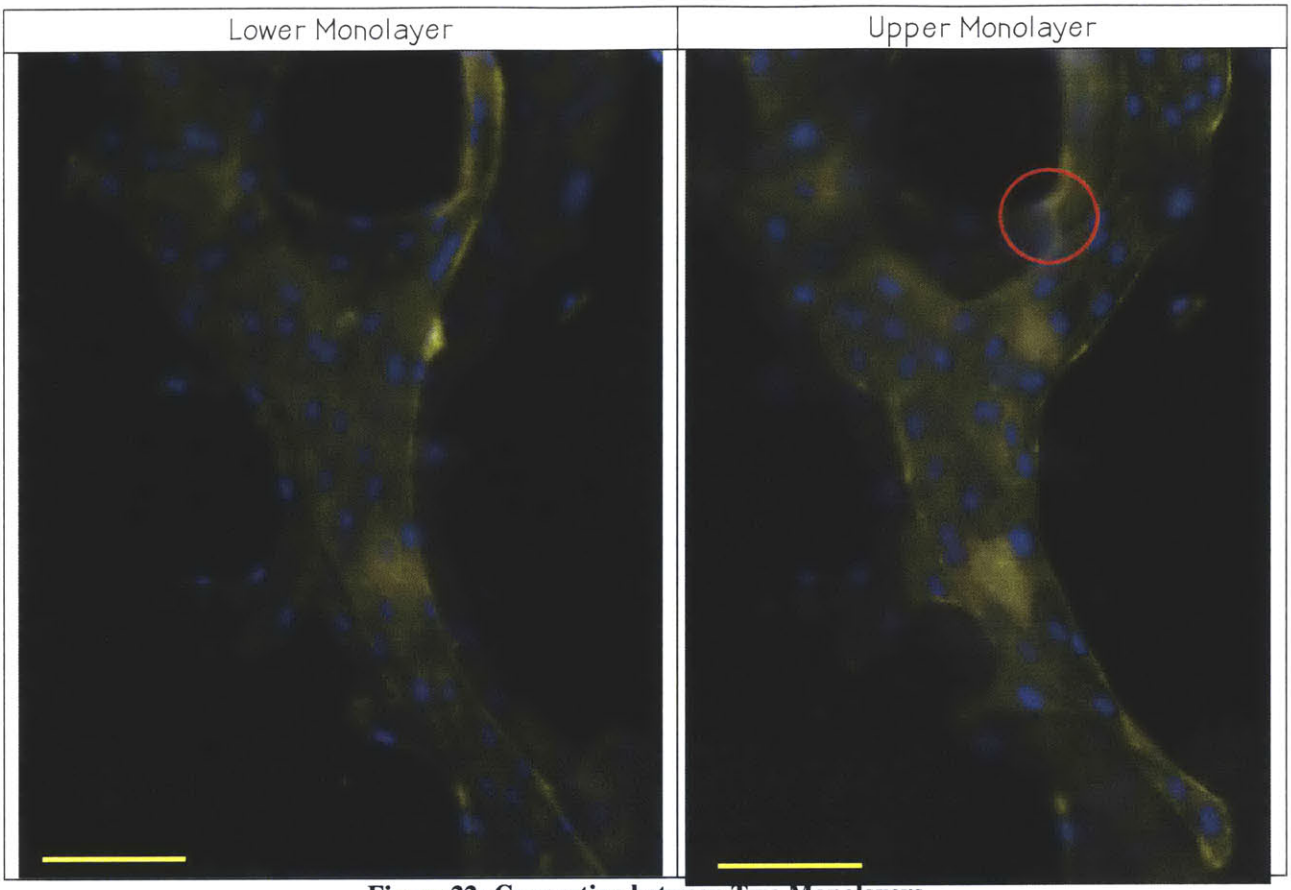

Figure 22: Connection between Two Monolayers
The connection is circled in red. The actin stain clearly shows connection between the two monolayers. Scale Bar: 100μm

An image was taken every 1μm in the z-direction for 100μm and the images were later deconvoluted and stacked. The schematic illustration describes the geographic correlation in different parts of each picture. For (A), the large image on the top left represents the image in the xy plane, the monolayer plane. The right portion of the image is the reconstructed image in the xz plane and the bottom portion in the yz plane. The white lines determined the focal point. The blue dashed lines demonstrated possible connections through the sample. The connections all seemed to be very straight and this raised suspicion that they could simply be shadows and not real connections. Further evidence is needed to

resolve this issue. However, in support of these observations, it can be seen that some voids that do not connect the two monolayers are also observed, shadowed in the actin stain, as circled in pink. In (A), a clear circle can be observed in the xy plane. However, when the actin stain was observed in the xz plane, it didn't extend all the way across.

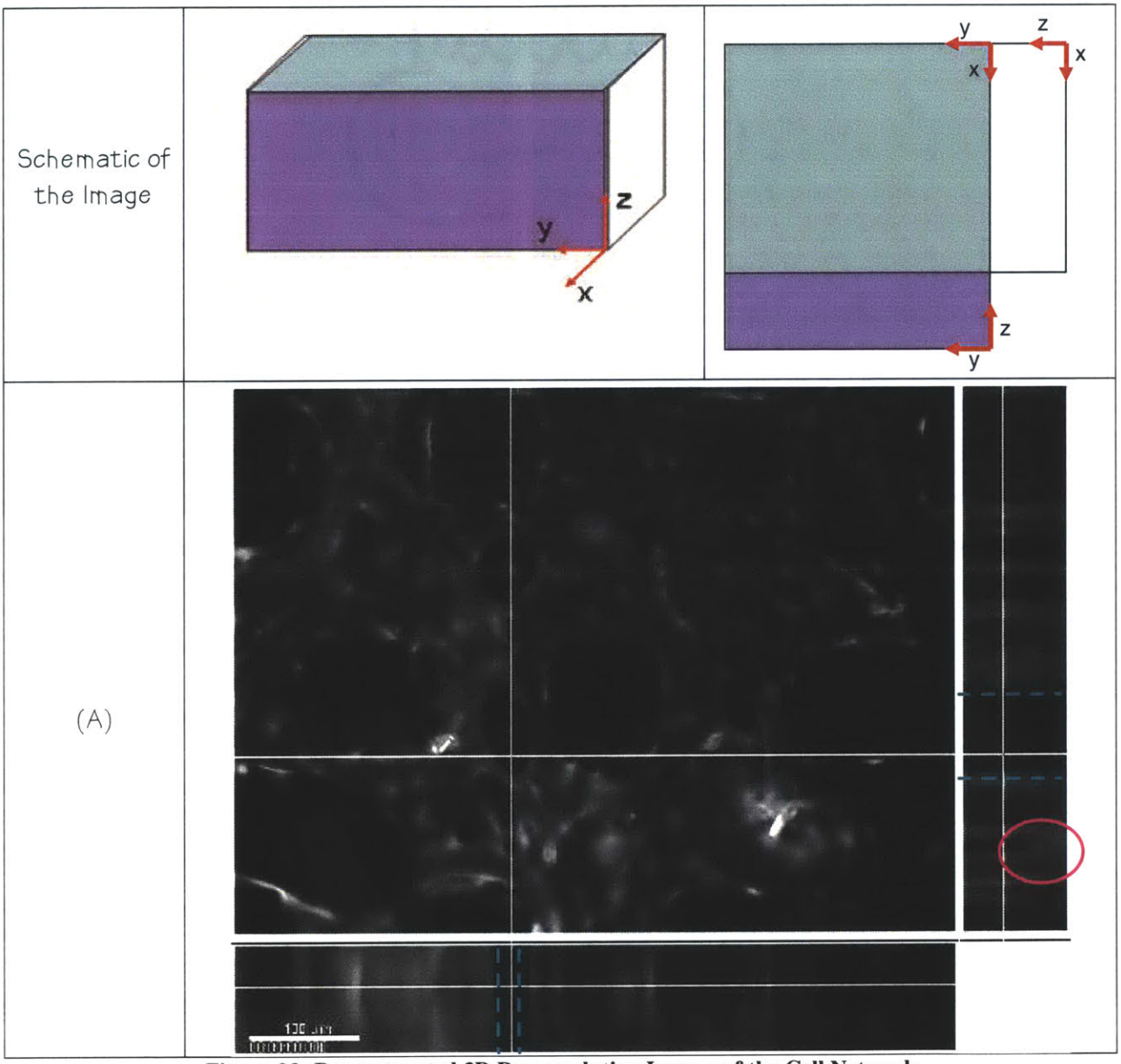

Figure 23: Reconstructed 3D Deconvolution Images of the Cell Network
Scale Bar: 100μm
The blue dash lines represent the through connections from one end to the other end, while the pick ellipse points out the voids that didn't extend all the way

Since it is difficult to decipher the possibility of a tubular structure through 3D reconstructed images, 2D images were taken every 5μm apart focusing on a targeted structure. The goal is to gain insights on the depth of the connections. From Figure 24, it can be seen that the actin "rim" was in focus for around 25μm. However, it is unclear whether multiple cells were connected in the z-direction.

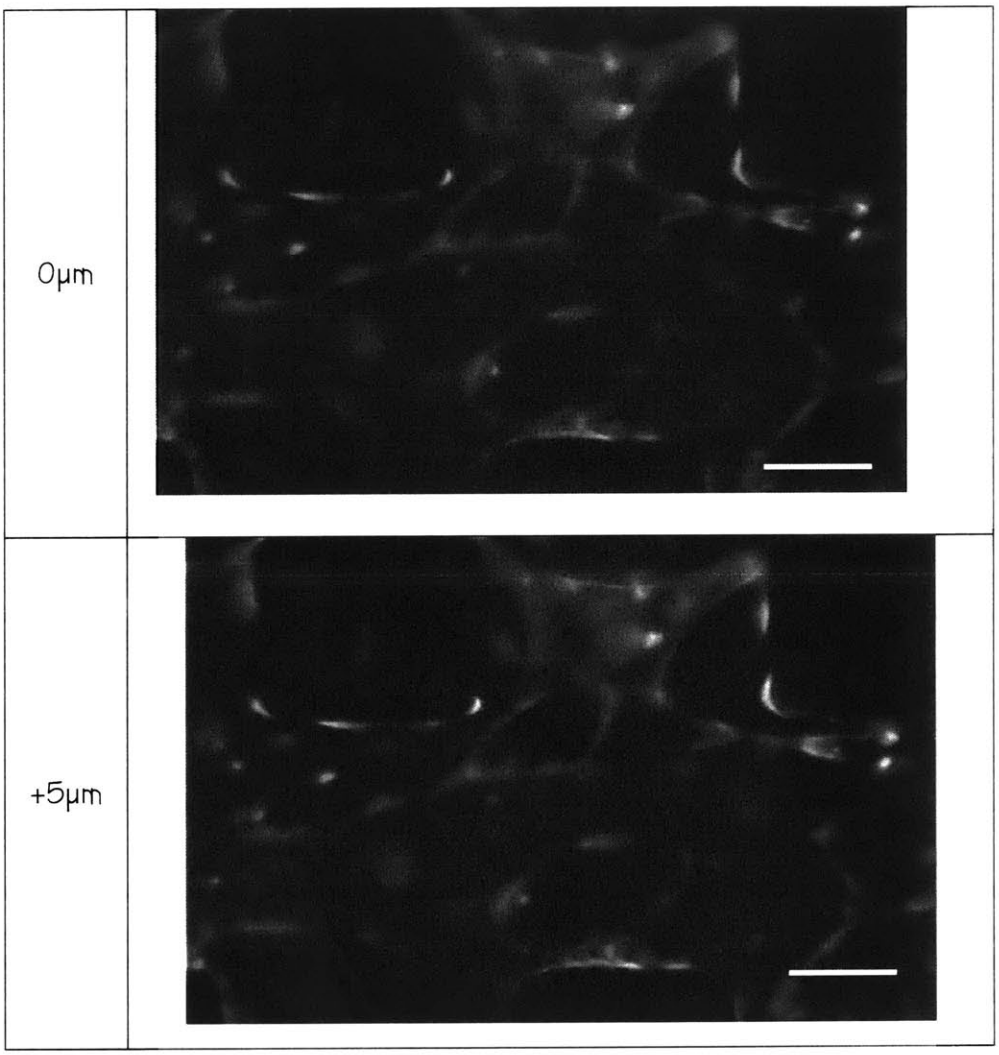

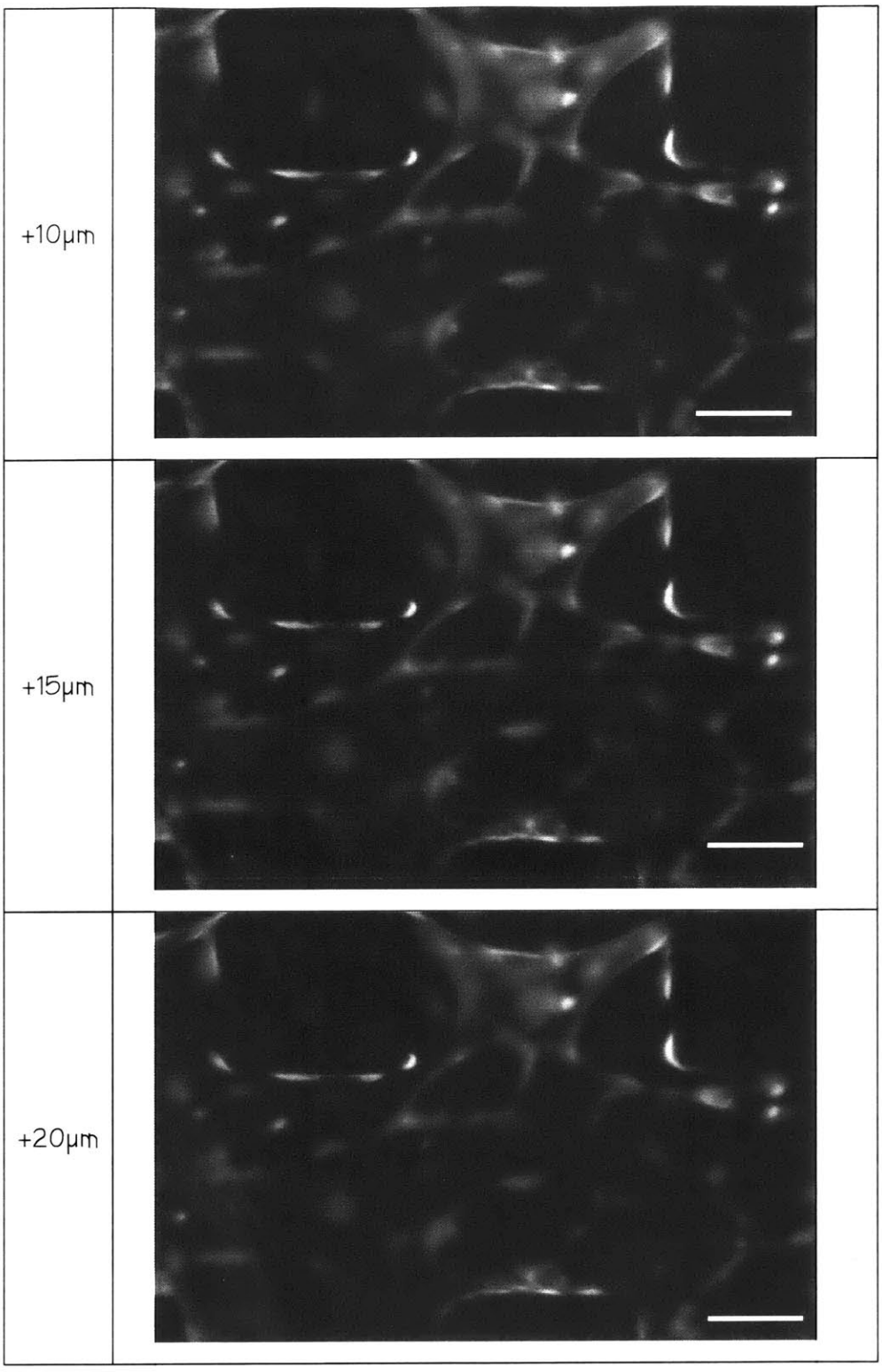
+10μm
+15μm
+20μm

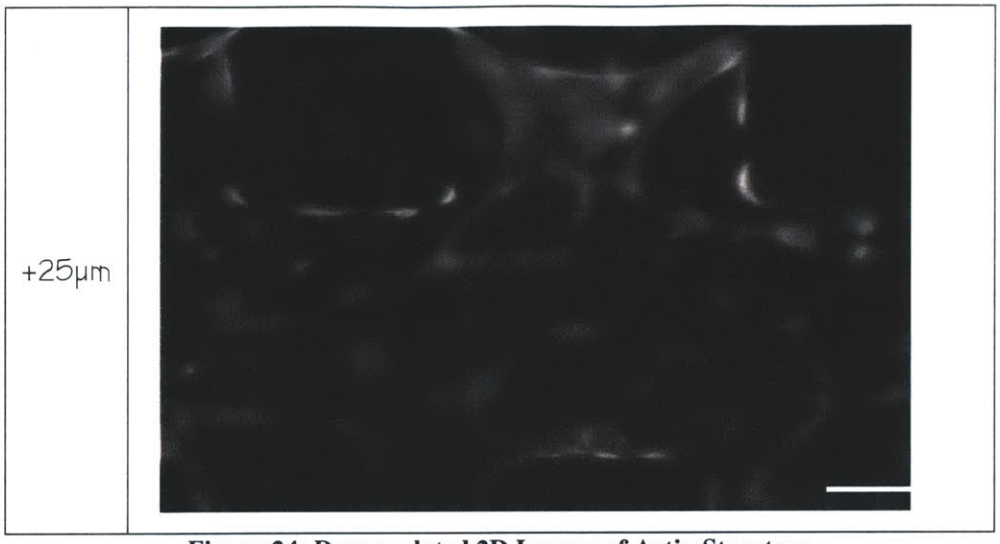

Figure 24: Deconvulated 2D Images of Actin Structure
Scale Bar: 50μm

4.2.5 Time Progression of Network

Both HUVECs and HMVECs continuously migrated everyday for the duration of the experiment. No regression was observed (Fig. 25). In this particular sample, it could be seen that the network reached across the gel cage in 7 days. To quantify the results, the average invasion area and maximum length were measured. The results showed that both the migration length and the invasion area increased with time. As for the different flow conditions, it did not prove to the statistically significant for either the invasion area or the maximal invasion length (Fig. 26 & 27).

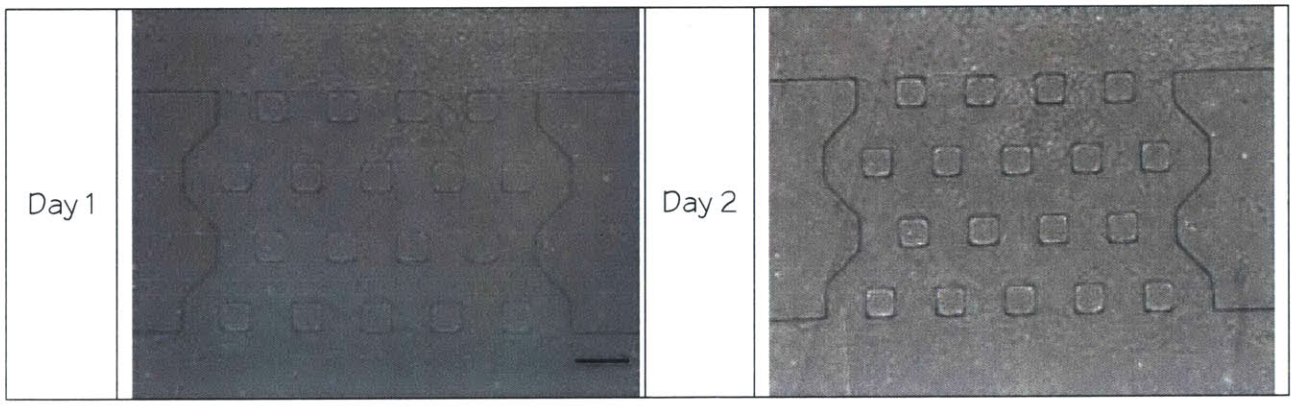

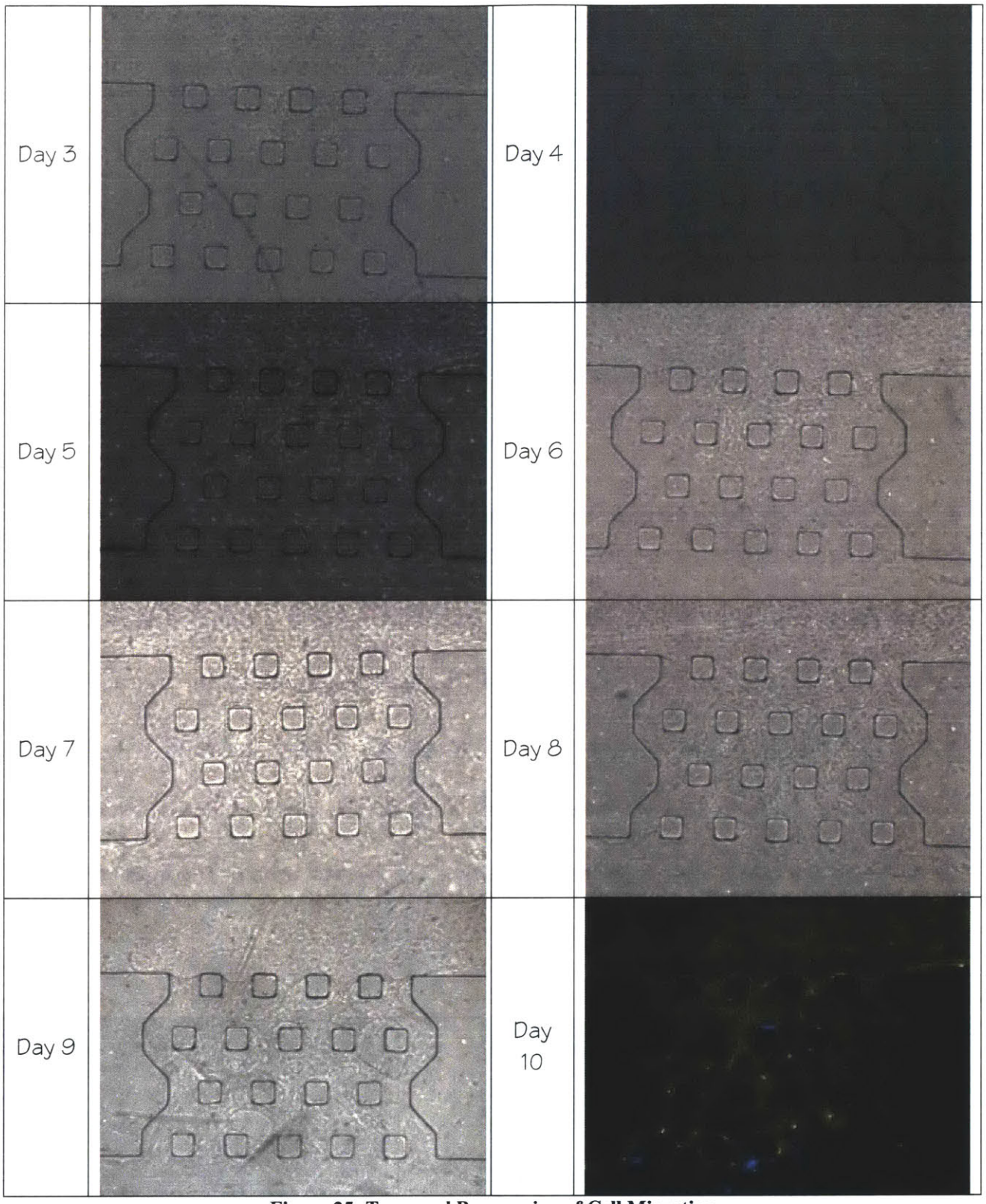

Figure 25: Temporal Progression of Cell Migration
Scale Bar: 200μm

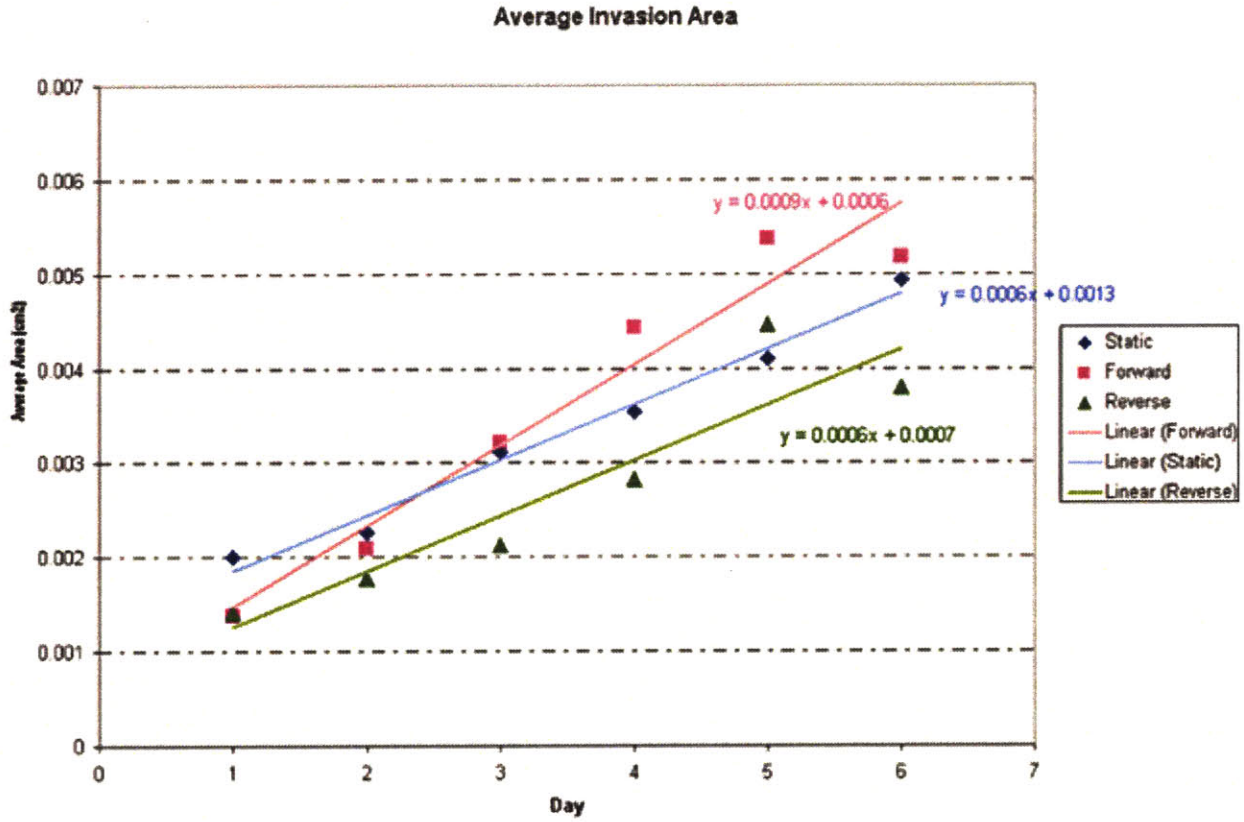

Figure 26: Average Invasion Area over Time

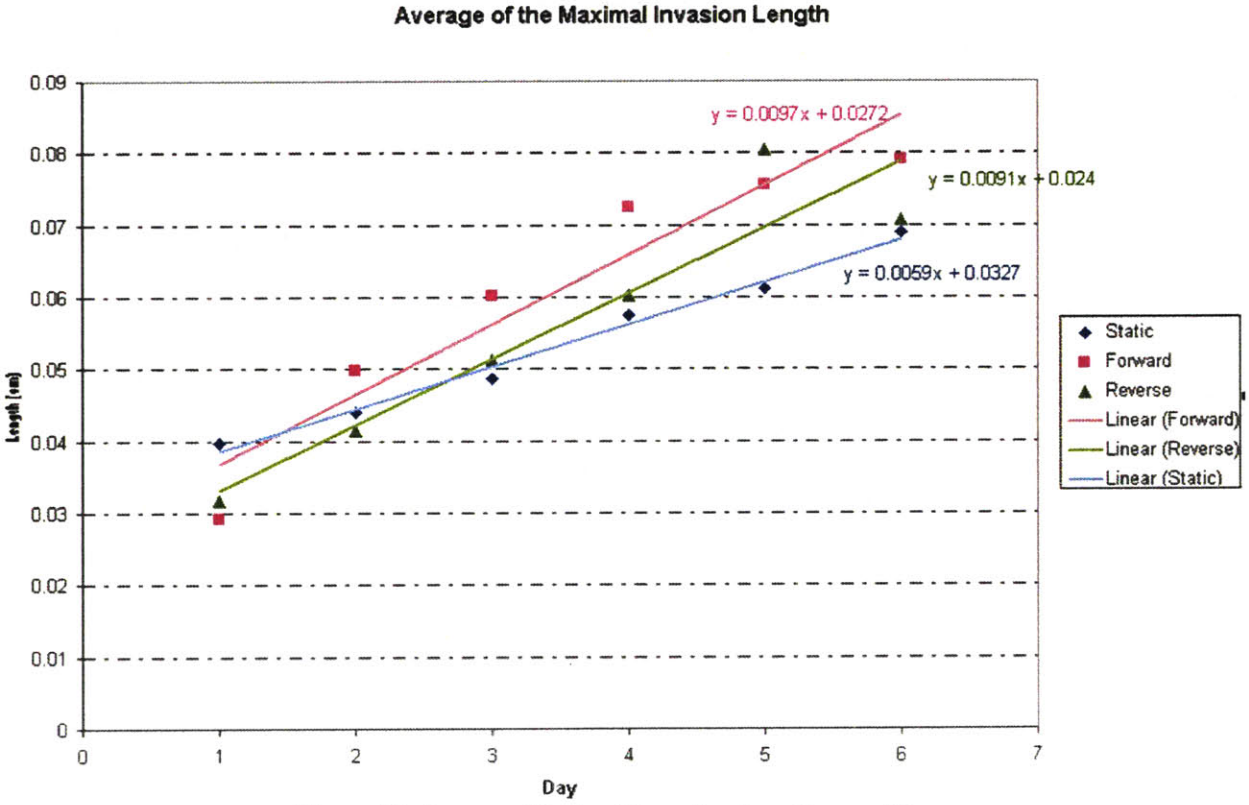

Figure 27: Average Maximal Invasion Length over Time

4.3 Two-Tiered Modeling

The complexity of experiments can sometime obstruct the fundamental transport problem. Therefore, a simple first order model was used to investigate the relationship between convection and diffusion both in between the endothelial cleft space as well as in the collagen scaffolding. At a low flow velocity, the interplay between convection and diffusion is important. In addition to altering the concentration distribution, flow may also impose mechanical stress upon the endothelial cells which induces mechanically activated signaling pathways. To gain insight into the effect of interstitial flow on both the transport phenomenon and the possibility of mechanotransduction, a first-order model was developed in both the cellular scale as well as the scale of the bioreactor. The scale of the bioreactor system is relevant for paracrine growth factors, such as VEGF. A two-tiered approach is taken. First, a model is developed on the length scale of the cell. Secondly, another model is used to model the concentration distribution in the gel. By equating the concentration and flux at the interface and other appropriate boundary conditions, the concentration distribution for both the interendothelial cleft space and the gel can be found.

4.3.1 Cellular Level Modeling

4.3.1.1. Mechanical Stress on the Endothelial Cell Wall

Interstitial flow imposed on the monolayer can only flow through the interendothelial cleft space assuming the cell body is impermeable. Other assumptions include:

1. Steady state,
2. Uniform endothelial cells monolayer

3. Neglect any effects from the junctional strands or glycocalyx
4. The endothelial walls are rigid and non-deformable
5. 1D transport
6. Locally fully developed flow in the interendothelial cleft space

By simple mass conservation, average flow velocity (U_{gap}) inside the gap is much greater than the imposed velocity (U_{apical}). With reasonable dimensions, U_{gap} is roughly 100 times higher than the apical velocity (which is imposed by either syringe pump or pressure head). Such drastic difference is unlikely. However, an increase in velocity inside the gap is not surprising. Therefore, for further analysis where the average velocity is needed, three values would be used, U_{apical}, U_{gap} and $(U_{apical}+U_{gap})/2$. The true effective average flow velocity in the interendothelial cleft space is likely to lie between U_{apical} and U_{gap}. Furthermore, by applying lubrication analysis, the velocity profile can be found in order to determine the stress on the endothelial walls (Eq. 6).

$$U_2(u,x) := \frac{w^2}{2\cdot\mu}\cdot\left(\frac{-\Delta P(u)}{h}\right)\cdot\left[\left(\frac{x}{w}\right)^2 - \left(\frac{x}{w}\right)\right]$$

Equation 6: Velocity Profile in the Interendothelial Cleft Space

$$\Delta P(u) := \frac{12\cdot\mu\cdot u\cdot h}{w^2}$$

Equation 7: Pressure Difference between the two Ends of the Cleft Space

u represents the mean velocity

$$\tau_{yx}(u,x) := w\cdot\left(\frac{\Delta P(u)}{h}\right)\cdot\left(\frac{x}{w} - \frac{1}{2}\right)$$

Equation 8: Shear Stress along the Wall of the Cell

Relevant values of shear stress, pressure difference are listed in Table 1. The known minimal shear stress on endothelial cell monolayer which elicits potential mechanotransduction

response is 10 dynes/cm^2. If U_{apical} is used to calculate shear stress, one would assume that mechanotransduction would not play a role in the cell behavior. However, the expedited flow velocity in the gap increases the shear stress along the wall and thus mechanotransduction might be important even when a low value of interstitial flow is present.

	ΔP [Pa]	τ_{yx} at the wall [dyne/cm^2]
U_{apical} (10μm/min)	14.7	0.49
½ (U_{apical}+U_{gap}) (582μm/min)	855	28.5
U_{gap} (1154 μm/min)	1696	56.5

Table 1: Pressure and Shear Stress at Various Velocities

4.3.1.2 First Order Transport Phenomenon in between the Interendothelial Cleft Space

This model attempts to describe the transport process with interstitial flow in the interendothelial cleft space. Figure 28 is the schematic of the model.

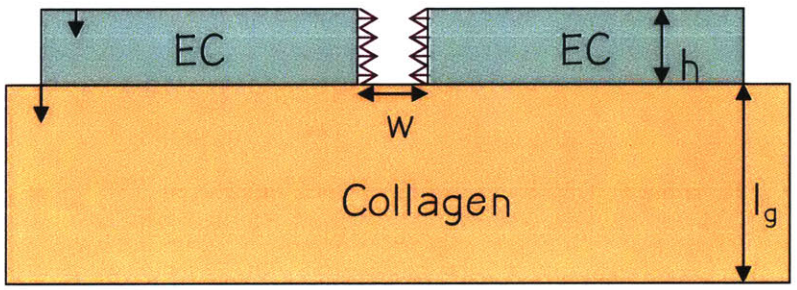

Figure 28: Schematic of the Transport in the Interendothelial Cleft Space (Not Drawn to Scale)

The assumptions of the model include those previous stated and also:

7. No homogeneous/bulk reaction
8. No binding (autocrine phenomenon is neglected)

9. Constant shedding rate of the growth factor from the cell along the gap only, and no shedding from the apical or basal surface of the cell

The Governing Equation of the System is

$$\frac{d^2}{dy^2}C(y) - \frac{u}{D}\cdot\frac{d}{dy}C(y) = \frac{-2\cdot r}{w\cdot D}$$

Equation 9: Governing Equation of the Transport in the Interendothelial Cleft Space

u is the flow velocity [m/s], D is the diffusion coefficient [m^2/s], r is the shedding rate of the growth factor produced by the cell [mole/m^2-s] and w is the width of the cleft space.

The boundary conditions are as follows,

At y = 0, C(y=0) = C_media

At y = bottom of cell, C (bottom of cell) = C (Top of gel)

At y = bottom of cell, the flux, N, matches at the interface.

N(bottom of cell) = N (top of gel)

Figure 29 shows the four concentration profiles in between the interendothelial cleft space examined in the model: 2 different gel cage size (5mm and 1mm). The model is aimed to estimate the concentration profile distribution in between the endothelial cell cleft space. The three different lines represent the three different cleft space widths. The red line represents the narrowest gap (20nm) and the green dashed line is the widest one. The difference in concentration from the apical and the basal surfaces decreases as the cleft space becomes wider. This difference, however, might be the potential mechanism for cell polarization.

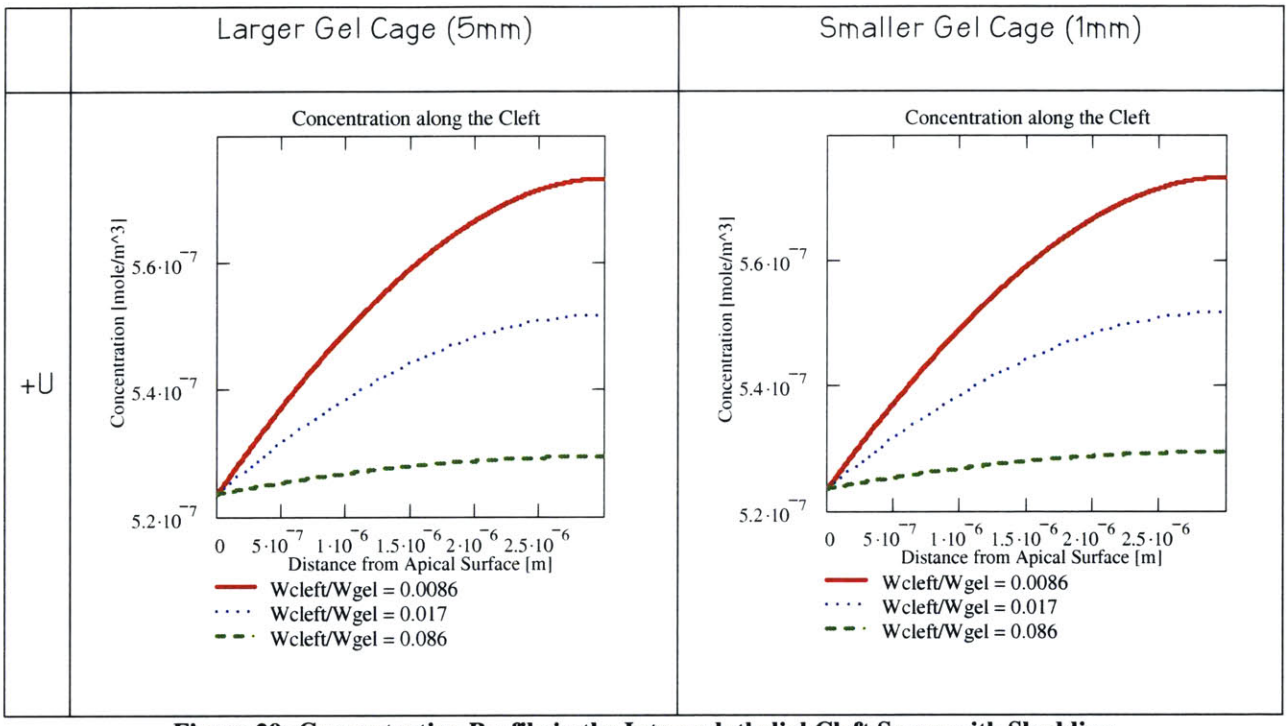

Figure 29: Concentration Profile in the Interendothelial Cleft Space with Shedding
The values used to plot this graph: D = 7E10^{-7}cm^2/s;
w = 20nm when walls are assumed rigid; h = 3μm;
C_media = 5.2*10^{-10}M ; r = 10^{-14} mole/m^2-s

4.3.2 Bioreactor Scale Modeling

The governing equation is

$$\frac{d^2}{dy^2}C(y) - \frac{u}{D}\cdot\frac{d}{dy}C(y) = 0$$

Equation 10: Governing Equation of the Transport in the Gel

In the meso-scale bioreactor, the length of the gel is modeled as 5mm (Fig. 30). As seen in the figure, the concentration is constant for most regions of the gel. The red line describes the velocity profile if the cell wall is completely non-deformable while the blue and the green line explains the velocity profile when the cell wall is deformed (taken into account by the increase in w, width of the cleft space).

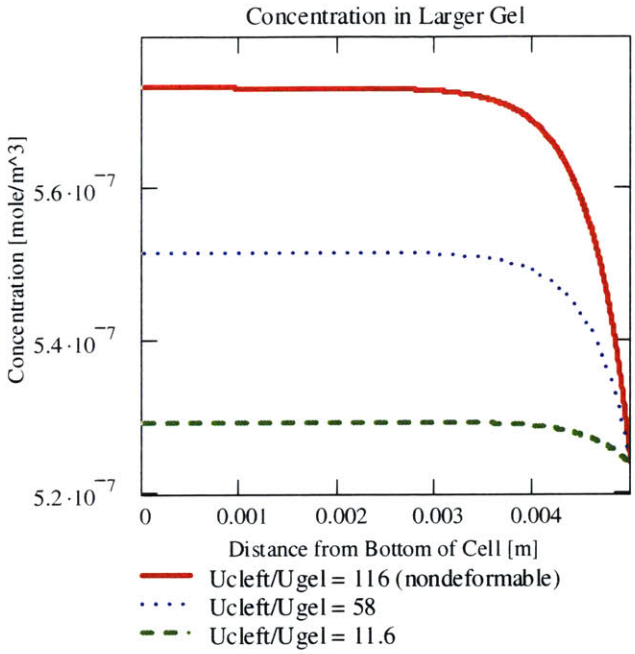

Figure 30: Concentration Distribution in Gel in Meso-scale Bioreactor with Shedding

To model the same phenomenon in the microfluidic device, the gel length is reduced to 1mm. The effect is quite dramatic for the concentration profile in side the gel. The concentration distribution is parabolic and a gradient can be observed (Fig. 31). This suggests that the shedding of growth factors from the cells can create a gradient which decreases as the distance increases. In other words, a concentration gradient is more likely to occur in a smaller gel region than a larger one if a concentration source, such as growth factors secreted from cell monolayer, is present.

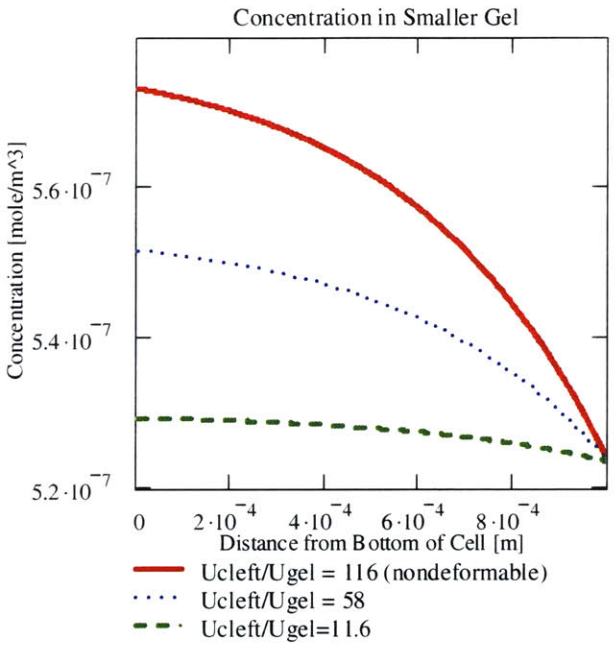

Figure 31: Concentration Distribution in the Microfluidic Device with Growth Factors Shedded from Cells

5. Discussion

5.1 Meso-Scale Bioreactor

The meso-scale bioreactor was a simple and direct way to investigate the capillary morphogenesis process. In most experiments with the transwell system, only the monolayer is observed. The meso-scale bioreactor design enabled observation of the gel and sprouts from the side so sprouts could be better imaged. PDMS wall allowed for great gas permeability. There were, however, several challenges with the meso-scale bioreactors. The thin PDMS wall tended to deform easily, especially when flow was applied. Gel would detach from the thin PDMS wall and flow would flow through between the PDMS and the collagen gel. Another challenge was the low survival of the static/low flow rate culture when cells were suspended in the gel. In this case, little nutrient was initially present in the collagen gel, and nutrient-rich medium was on the two ends of the bioreactor. Since diffusion was the only means for cells to receive nutrient under static condition, the large length scale might starve cells severely. With an order of magnitude estimate, the time scale for a small molecule, such as VEGF ($D = 7x10^{-7} cm^2/s$) to reach over 3mm by diffusion would be

$$T_{diffusion} = L^2/D = 35hr$$

By the same token, it would take a long time for wastes to diffuse away. The scale of the system was much larger than the length scale of interest and this posed as a problem for fine control of the microenvironment. The thickness of the collagen gel and the opacity of PDMS often hindered the quality of the direct observation. In addition, when fixed gels were

removed from the system and placed on coverslips, it is unclear whether the internal cell network structures have been altered or not.

Nevertheless, from the meso-scale experiments, a surprising result was observed which hasn't been reported *in vitro*. When capillaries sprouted, it appeared to preferentially occur against the flow direction. Since this result was unanticipated, we decided to pursue it further to make sure it was not an artifact based on the device. Therefore, we used a microfluidic device to investigate if the same phenomenon could be observed. The discussion of the results from the microfluidic device will be presented in a latter section. In the following sections, I will focus on the findings from the meso-scale reactor and the effects of several variables examined experimentally.

5.1.1 Effect of Flow

In all three setups (cell monolayer, monolayer sandwiched between two layers of collagen scaffolds, and cells suspended in collagen gel) described in the Results section, the presence of flow enhanced cell survival. This is probably, at least in part, due to expedited transport compared to diffusion alone. In addition to cell survival, more sprouts were observed when the flow was present. Several key variables were examined with flow, such as the magnitude and direction.

5.1.1.1 Effect of Magnitude of Velocity

In previous studies by Semino and Hernandez, it was shown that capillary morphogenesis as well as Src phosphorylation both peaked at an interstitial flow velocity of around 10μm/min.

Those experiments were performed with the endothelial cell monolayer on top of the collagen scaffold and in direct contact with the media. 10μm/min did not induce capillary morphogenesis for the collagen sandwich or the cell-suspended experiments. Instead, ~50μm/min flow was necessary to induce capillary morphogenesis. Although we cannot know for sure, we suspect this to be due to the differences in signaling when cells are exposed to ECM on the basal side only versus surrounded by ECM. Cells needed to be polarized in order to sprout. By surrounding the cells with ECM three dimensionally, the polarity of the cell might be lost. The phenomenon of reorganization of the monolayer when sandwiched between two collagen scaffolds was not observed when cultured on a single layer of collagen. This led to the hypothesis of different signaling pathways in the two scenarios. To fully explore this problem, detailed signaling pathway studies need to be performed.

5.1.1.2 Effect of Direction of Flow

The hypothesis was to examine if chemotaxis is the main mechanism for capillary sprouting and cell migration. From the first-order modeling, it was observed that the chemical gradient decreases as the distance to the monolayer increases regardless of the flow direction. This will indicate that, if chemotaxis is the key mechanism, direction of spouting is not dependent upon the flow direction. However, experimentally, the sprouts appear to have a preferential direction against the flow when the monolayer was sandwiched between two collagen gel layers. In the case of cells suspended in collagen gel, no sprouts were observed. Nonetheless, individual cell migration also appeared to move against the flow direction.

These findings were contrary to the current literature. However, if one studies more closely, the differences in experimental/modeling setup can be the explanation of the apparent opposite findings.

A synergistic effect of VEGF and interstitial flow was observed downstream of the flow direction through transport simulations.[49, 55] In this particular model, VEGF is tethered to matrix and released as MMP is transported through ECM. In my experiments, growth factors were present in an endogenous form. As a result, the synergistic effect will not be applicable to the experiment. Another example of migration along the flow direction was observed during lymphoangiogensis. Although both lymphatic system and cardiac vascular system are both formed by endothelial cells, the nature of the cell type can be drastically different. [59]

One possible explanation of the phenomenon observed in my experiments can be the gradient of waste as well as nutrient created by the flow. Under static/low flow velocity conditions, the monolayer alone or monolayer sandwich experiments had good cell survival. This indicates that waste or nutrient diffusion is not the limiting factor. However, as the fluid flows through the monolayer, the waste created by the cell was also carried downstream creating a "more toxic" environment. On the other hand, the reservoir of fresh media is much bigger than the amount of media in the meso-scale device. Thus, the assumption of constant concentration of nutrient in upstream can be made. As the media flowed through the monolayer, nutrients were being consumed. In other words, a decreasing gradient of nutrient is expected based on these assumptions.

Another effect to be considered is the MMP gradient which changes the relative stiffness of the downstream and upstream collagen scaffolds. Endothelial cells produce MMP digesting the extracellular matrix to allow cell migration. The flow will generate a higher concentration of MMP downstream. Therefore, the downstream gel could be softer.

To fully test out these effects, better controls need to be made. For instance, in order to study whether the preferential migration is because of the increasing waste concentration or decreasing nutrient concentration, ammonia concentration can be tested at various locations or conditioned media could be used. To test whether gel stiffness plays a role in the directional spouting/migrating behavior of the endothelial cells, MMP-inhibited endothelial cells can be used and the gel stiffness can be varied in a controlled manner such as changing the concentration or the pH during polymerization.

5.1.2 Effect of Growth Factors/Serum

In addition to the mechanical effect of flow, chemical factors, such as VEGF and serum, also had a significant impact on the endothelial cell behavior. Systemic study was done for cells suspended in collagen gel. Key findings include: 1) HUVECs tend to survive better than HMVECs under static conditions regardless of the serum level, 2) higher serum level improved the survival of HMVECs while the survival of HUVECs appeared to be independent of the serum level and 3) VEGF was essential for cell survival. These observations were consistent with the relevant literature. If the effect of growth factors or serum level is to be

studied further, a multi-variable design of experiment needs to be performed along with flow to investigate whether there will be any synergistic, additive or competing effect.

5.1.3 Effect of Cell Seeding Density

Initial cell seeding density proved to be an important parameter as well, especially in the case of cells suspended in 3D. Better networks were found at higher cell seeding density. At higher density, cells are more likely to initiate cell-cell communication and possible paracrine interactions, and thus form networks. When studying network formations of endothelial cells in 3D, it was found that $1.5x10^6$ cells/ml is necessary to observe network formation. The initial cell density is noteworthy because the appropriate cell seeding density is quintessential in the appropriate cell behaviors.

5.2 Microfluidic Device

The rationale behind using the microfluidic device was that the results found in the meso-scale bioreactor appeared to contradict the current *in vitro* results. Therefore, we would like to reduce the device dependency and artifacts. The microfluidic device also allowed for imaging from the side of the collagen gel to conveniently observe the endothelial cell invasion process. Because of the glass coverslip, instead of PDMS, as well as the small height, the image quality of the microfluidic device is much better than that of the meso-scale bioreactor. Furthermore, because the scale of the device is closer to the scale of interest, the microenvironment is presumed to be better controlled. Several challenges associated with the microfluidic device include: 1) leakage which sometimes happened

between the coverslip and the PDMS device, 2) the varying pressure head and 3) the phenomenon of cell migration overwhelmed the endothelial cell sprouting due to extensive gel contraction. The microfluidic device was a useful tool to study cell migration in both 2D and 3D.

5.2.1 Effect of Direction of Flow

The direction of flow appeared to not make a difference on the extent of cell migration or capillary morphogenesis in this experimental setup. There can be several explanations.

First, when cells were initially seeded, they were placed on one side of the channel and a monolayer was formed as shown in Fig 32. As cells migrated into gel and contracted, a small gap was created between the collagen gel and the coverslip and another between the gel and PDMS as shown. Cells formed monolayers along the gaps. As a result, the intended flow direction no longer served the same purpose. As long as gaps were present, the flow would more likely go through them. The interstitial flow intended for the experiment will partially become the shear flow along the monolayer. It would be difficult to tease out the effects of shear flow from interstitial flow.

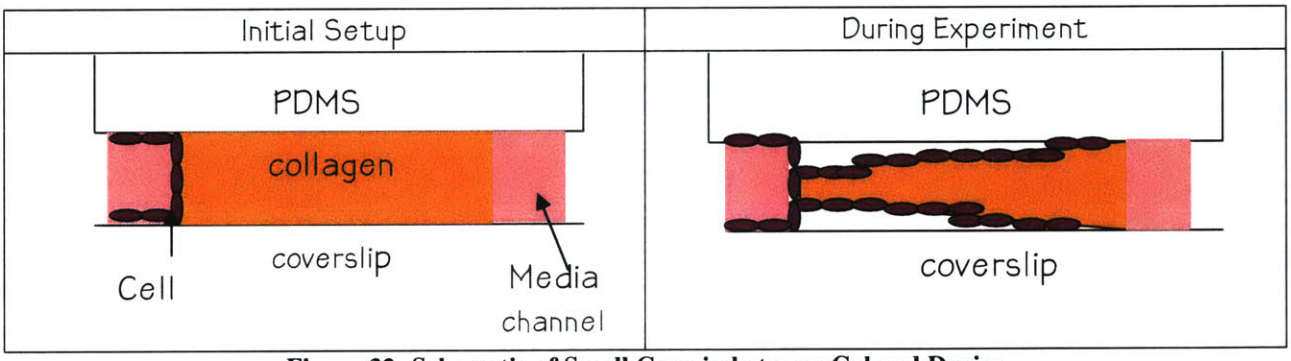

Figure 32: Schematic of Small Gaps in between Gel and Device

Secondly, all the experiments were performed under the baseline condition. In other words, no additional growth factors were added in either the endogenous form or the matrix-tethered form. There is the possibility that the effect of flow is only prominent when additional growth factors, such as VEGF, are added. To test this additional hypothesis, a series of experiments with different chemical microenvironments is to be performed. For example, a set of experiments will consist of 4 different conditions: no flow/no VEGF, with flow/no VEGF, no flow/with VEGF and with flow/with VEGF. By analyzing the results of these four scenarios, we would be able to gain insights of whether the effect of VEGF and flow is synergistic or additive and how important is the role of VEGF relative to flow on capillary morphogenesis.

Third, when studying the effect of flow in a small system, it is important to consider the interplay between diffusion and convection. A characteristic parameter to study such relationship is the Peclet Number (Pe) defined as

$$Pe = UL/D$$

U being the characteristic velocity, L the characteristic length and D the bulk diffusion coefficient. If Pe is much greater than 1, it means that convection plays a much more important role compared to diffusion. On the other hand, if Pe is much smaller than 1, diffusion is the dominant effect of the transport phenomenon. In this system, assuming that the growth factors behave as paracrines and transport through the monolayer into the gel, the appropriate characteristic length would be the gel cage width to study the how the flow affects the chemical distribution. In the microfluidic device, the length scale is smaller than

that in the meso-scale bioreactor. Therefore, the effect of convection is less significant in the microfluidic device assuming velocity and diffusion coefficient remain the same. If the correct comparisons are to be made for the two devices, the peclet number should be held constant for the both experiments. Therefore, fluid velocity should be higher in the microfluidic device.

Furthermore, the contraction of the collagen gel may have a significant impact on the flow distribution and the effect of it. The contracted gel is much more permeable to flow than the gel with little contraction. The contraction may also cause detachments of the gel from the PDMS or the coverslip surface which leaves gaps with much less resistence to flow. This phenomenon will make the "true" interstitial flow through the gel much lower since most of the flow will go through the gaps. It will also be close to impossible to evaluate what the values will be. Therefore, if the experiments are to be repeated and analyzed further, a stiffer gel which is less likely to contract should be used. 2mg/ml collagen from BD Biosciences has been found not to contract greatly from similar work done in our laboratory by Vernella Vickerman. In these experiments, the collagen stock was from a different source, Upstate. It appeared to be less stiff than the gel from BD Biosciences at the same concentration (Fig. 34). Although the exact reason is unknown, it is important to note the differences of the collagen stock from various suppliers. For a systematic study, one source of gel should be used at various concentrations to determine the optimal concentration to study capillary morphogenesis.

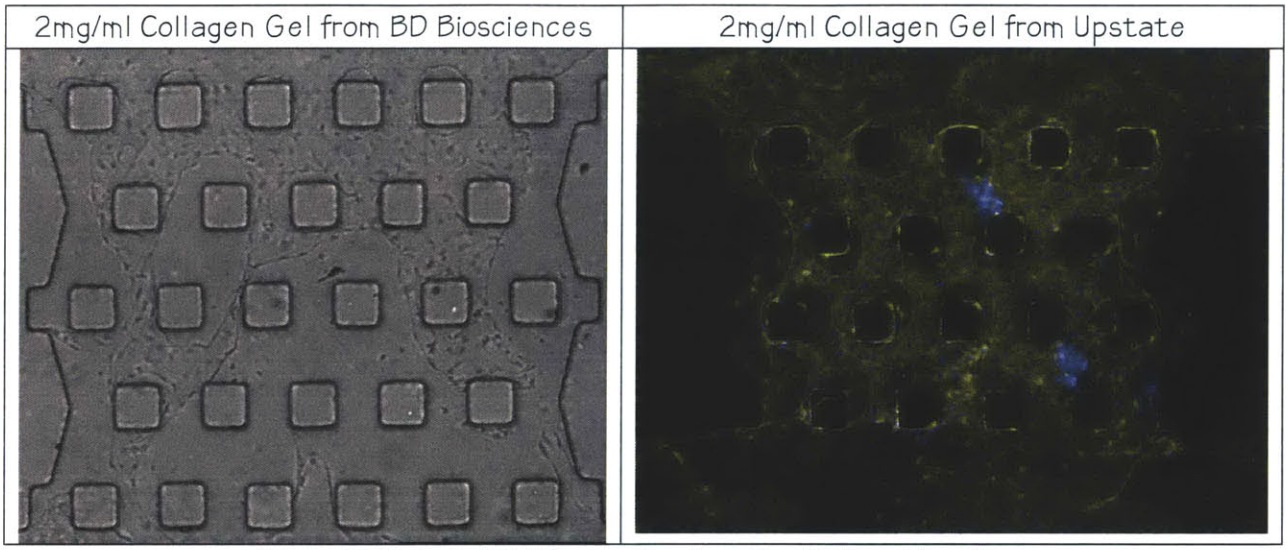

Figure 33: Extent of Gel Contraction from Two Different Suppliers

5.2.2 Formation of Multiple Monolayers

As described in the previous section, at least two monolayers were formed as cells migrated into the gel region, one in each gap space. However, sometimes, three monolayers were observed. It is unclear of the exact location of the 3rd monolayer. Since more of the images showed that the cells on the monolayer displayed a two-dimensional morphology, the collagen gel might have formed some planar crack which allowed cells to migrate into. The z stack reconstructed images failed to provide additional information of where the monolayers were located relative to one another. However, the z-stack images were taken two weeks after the cells have been fixed. The action network structures appeared to have deteriorated over the 2 week period (Fig 35). This might explain the limited amount of information gained from the three-dimensional reconstruction images.

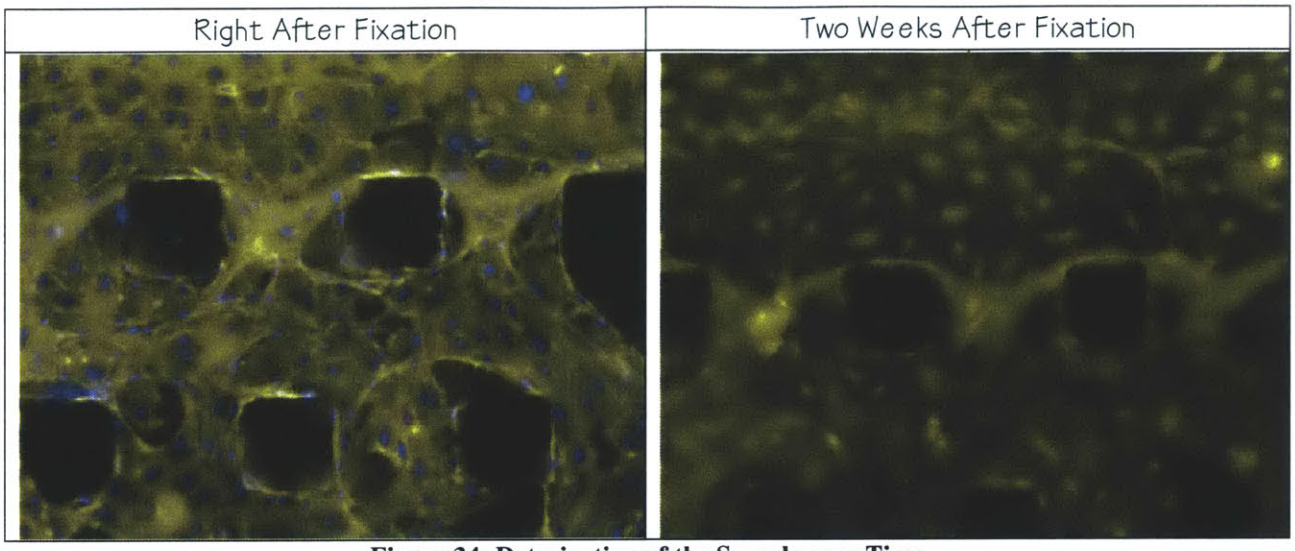

Figure 34: Deterioation of the Sample over Time

5.2.3 Connections between Monolayers

From analysis of 2D images of different depth, there was evidence of connections between the monolayers. The distance between the monolayers was around 80μm. This length is within the diffusion length scale. Therefore, it is expected that connections were found independent of the presence of fluid flow. Once the connections were observed in 2D images, the next step was to determine whether the connections possessed lumen and whether or not they were consisted of multiple cells. The 3D images, unfortunately, did not provide much further insight. From Fig. 24, multiple nuclei were observed for each ring-like structure that extended for roughly 25μm. It appeared that multiple cells connect together on one horizontal plane and extended downwards. It is unclear, however, that whether there were multiple cells lined up in the vertical direction.

5.3 Comparison of the Two Devices

Experiments were performed at two different length scales: one in the millimeter scale and the other in micrometer. The aim was to investigate the effect of interstitial flow in a device-independent manner. There were advantages and disadvantages to each reactor. The biggest challenge to overcome for the meso-scale bioreactor was the deformation of the PDMS walls. Leaks were often observed. Another challenge was the poor optical quality due to the opacity of PDMS and the thickness of the gel. The flow was driven via a syringe pump which allowed for precise flow velocity. However, there was no way to predict the pressure distribution inside the device. The medium was kept in a syringe outside of the incubator. This may influence the biocompatibility of the media. On the other hand, the challenges associated with the microfluidic device were the contraction from the collagen gel away from the coverslip and the PDMS, and the difficulty in producing a tight seal between PDMS and the coverslip. In addition, the pressure difference was kept with 200µl pipet tips with different amount of media. Two problems emerge from such a setup: the constant change of pressure head and the effect of evaporation. The tapered nature of the pipet tip made the estimation of the effect of evaporation especially difficult since the exposed area changes depending on the height of the media. During the later time points of the experiment, it was difficult to maintain a pressure head over 24hours. The highly permeable contracted gel made the entire system much less resistant to flow.

If comparisons between devices were to be made, the challenges mentioned above need to be overcome to study the phenomenon better. In addition, dynamic similarities need to be

taken into account. In other words, in this setup, the important parameters include the Peclet number, a reaction term which takes into account of the effect of reactions compared to diffusion or convection. A model described in the next section is developed to address the potential difference the size of the bioreactors.

5.4 Modeling

Although the model made some assumptions that are far from reality, such as rigid cell walls, it still provided some insights on how the flow might have an effect for both the possibility of mechanotransduction and the transport of growth factors.

In the aspect of mechanotransduction, monolayers are generally impermeable. When a flow is imposed, by mass conservation, the flow must go through the monolayer. Assuming that the cells are not permeable, all the fluid will pass through the interendothelial cleft space. The shear stress imposed on the walls of the cell junction is greater than 10 dynes/cm^2, which is commonly known to induce mechanotransduction response. If the cell walls are to deform realistically, the stress predicted by the model will overestimate the true stress imposed on the wall. Junction strands are neglected in the model. It is perceivable that the strands and cadherins play important role in the stress distribution in the cleft space. In addition, the endothelial cells in the monolayer are not rectangular in shape as it is in the model. Rather they general spread flat toward the edges of the cell on 2D.

To look at the transport phenomenon in the interendothelial cleft space, the assumptions of the constant concentration at the top of the cell and the bottom of the gel can be made because of the large reservoir connected on both ends. By simply applying two more

boundary conditions of matching flux and concentration at the interface, the two concentration profiles can be found. In this model, two questions were examined. First, how the concentration profile will change in the interendothelial cleft space by varying the width of the cleft and secondly, how will the concentration distribution be altered when the scale of the gel cage varies. To answer the first question, it is crucial to understand the relative importance of convection and diffusion. Pelect number is ~1 at the narrowest gap (20nm) and decreases with increasing gap space. This means that diffusion is dominant as the cleft space becomes wider. Intuitively, widening cleft space describes larger volume in the cleft space. As a result, the shedding of the growth factors will have less effect on the concentration profile.

The model also found that the shedding of growth factors from the cell monolayer can induce a gradient inside the collagen gel. The concentration gradient is more prominent if the gel cage region is shorter. Concentration decreases in the gel as the distance away from the cell monolayer increases regardless of the flow direction.

In addition, if binding reaction term is added in the model, the model can be used to look at autocrine signaling. However, it is not included in the current model because what we are interested in is the paracrine signaling which distributes through the gel.

By this two-tiered approach, I was able to find out the effect of the size of the reactor on the distribution of the morphogen in the sytem. What is found through the model is that when the gel size is larger (5mm), the concentration distribution is relatively flat through the gel. However, when the gel size is smaller (1mm), the concentration distribution showed a

gradient from the bottom of the cell to the other end of the gel. This demonstrated that if we treat the monolayer as a source of growth factors, it will create a chemo-gradient along the gel in a smaller gel cage. To apply this finding to the experimental results, it showed that the effect of chemo-gradient inside the gel is likely to be less prominent in the meso-scale bioreactor compared with the microfluidic device.

The model also provided some insights on the potential mechanism of cell polarization under flow. By examining the concentration profile inside the interendothelial cleft space, a ~10% concentration difference can be observed from the top of the cell to the bottom of the cell. This gradient can be used to explain the polarization of the cell. However, the model does not provide a solid evidence of this effect or disapprove other mechanisms which can cause polarization.

6 Conclusion

The motivation behind this master's thesis was to determine the optimal physical condition for capillary morphogenesis. In particular, interstitial flow has been shown to influence capillary morphogenesis. 10μm/min flow velocity appeared to be optimal for capillary morphogenesis. However, the direction of flow has never been examined thoroughly. Furthermore, with the current literature, there has been contradicting results *in vivo* and *in vitro*. With this work, two different experimental setups were used, one in the meso-scale (mm), and one in the micrometer scale. What I found was that capillary sprouting and cell migration appeared to preferentially move against the flow direction in the meso-scale bioreactor. The same trend was not found for the microfluidic device in the baseline experimental setup. Several phenomenons can be used to describe the discrepancies. First, the gel contracted greatly in the microfluidic device probably because of the different supplier of the collagen stock solution. The more permeable gel made the flow conditions much more difficult to control. Secondly, the smaller scale of the microfluidic device will make diffusion more important than convection for the paracrine growth factors.

The project is the first step into investigating the potential device dependencies of experiments examining capillary morphogenesis under interstitial flow. Because of the complex nature of the cell behavior in 2D and 3D, two different scenarios were observed in the two experimental setups. If the work is to be continued, the natural progression would be first to alter the experimental conditions of the microfluidic device so that 3D invasion is to

be observed. In addition, a similarity analysis might be considered if the results from various devices are to be compared.

Appendices

Appendix I : Protocol of Microfluidic Device Setup

Sterilization

1. Autoclave devices, water, and hydration box for *20 minutes on the liquid cycle*
   (a) Add 250 ml water in glass beaker and cover with aluminum foil
   (b) Add ~200 ml of water to the bottom of a pipette tip box and assemble. This will later be used as a humidifier for the devices while gelling
   (c) Drop devices into a large flask/jar with water in it and cover with aluminum foil
   (d) Place all items in a plastic tub

2. Autoclave devices for *20 minutes on dry cycle with 10 minutes dry time*
   (a) Place devices in a pipette tip box (not the ones autoclaved with water)
   (b) Place Glass cover slips in a separate pipette tip box
   (c) Leave devices in autoclave for ~ 5min following the end of the cycle to allow drying

3. Clean micro-syringe with autoclaved water in tissue culture hood
   (a) Add 5ml autoclaved water to a 15 ml vial
   (b) Place 2.5 µl micro-syringe tip into water and connect pipette tip
   (c) Turn on vacuum and draw sterile water through syringe
   (d) Leave vacuum on to dry syringe
   (e) Fill ~6 eppendorf tubes with sterile water to flush out syringe when adding gel

Plasma treatment for sterilization and hydrophilicity

1. Turn plasma sterilizer on during the dry autoclave cycle in order to allow it to warm-up (located in 4th floor ISN lab – see Marco for access)
2. Bring clamp, paper towels, 70% ethanol, glass slides and stop watch with you to ISN
3. Wipe all surfaces surrounding machine with 70% ethanol
4. Retrieve devices from autoclave and start cell passage (see next section)
5. Place devices on glass plate channel side exposed (2 per glass plate) and put in sterilizer
6. Hold vacuum front plate on sterilizer, turn on pump (make sure valve on front plate is closed), and start stop watch (leave running from the start of plasma sterilization until loading devices with gel to get an idea of how long hydrophilicity of PDMS lasts
7. Run vacuum for 2 minutes
8. Turn on irradiation to high and open valve slightly to adjust the color to a bright purple/pink
9. Leave irradiation on for 2 minutes
10. Retrieve devices and repeat as many times as required
11. Immediately return to tissue culture to mix collagen and load devices

Loading gel/cell suspension in device

1. Turn on laptop at tissue culture hood and open microscope icon (plus in microscope USB if not already done)
2. Fill syringe with 2.5 µl gel
3. Position device on a glass slide with channels up and 2 ports open to the air
4. Focus microscope on gel packing region (focus on grid)
5. Move micro-syringe manipulator in towards device until syringe tip come into field of view
6. Use micro manipulators to center syringe time over grid. Lever the joy-stick in neutral so you have some fine control while loading gel. Lower until syringe tip is in focus.
7. With one hand on the joy stick to keep syringe tip centered, use other hand to place one drop of collagen on device grid. If the surface is hydrophilic, the gel will wet the surface. Add 1 or 2 more drops until region is filled as determined by gel level reaching the top of the grid "posts"
8. Raise syringe and move away from microscope stage
9. Center a sterilized, round glass cover slip on the device. Do not press very hard. The cover slip will be secure
10. Place device in autoclaved micropipette box with water and place in incubator for ~ 30 – 40 minutes to allow gel to cure. When substituting media for water, the gelling time is slightly extended.

** Note: After filling 2 devices, syringe must be flushed with sterile water to prevent clogs. Pipette up and down sterile water from filled 1ml spider tube with syringe and then flush once with collagen gel. Use new sterile water each time.

11. After gelled, place 20 µl drop of media over each port opening for 24 hr incubation
12. Add media every 24 hours

Appendix II : MathCad Code for First Order Model

General Assumptions:

1. No Bulk Reaction
2. Monolayer of EC
3. Walls of Monolayer are Rigid
4. Steady State
5. Neglect the Effect of Glycocalyx
6. Neglect Effect of the Junction Strands

Parameters

Geometry

$h := 3 \cdot 10^{-6} m$ Height of EC

$w := 20 \cdot 10^{-9} m$ Interendothelial Cell Cleft Width

$l := 5 \cdot 10^{-6} m$ Half the length of EC

$b := 1.5 \cdot 10^{-6} m$ Half the depth of EC

Solute Properties

$$r_2 := 10^{-5} \cdot 10^{-9} \frac{mole}{m^2 \cdot s}$$

$D := 7 \times 10^{-7} \frac{cm^2}{s}$ Diffusivity of EGF

concentration in media (20ng/ml) MW of VEGF = 38.2 kDa

$$20 \cdot 10^{-9} \cdot \frac{g}{mL} \cdot \frac{mole}{38200g} = 5.236 \times 10^{-10} \frac{mole}{L}$$

Diffusion Only Case

$$C_1(r, l_g) := \frac{\left(\frac{r \cdot h^2}{w \cdot D} + \frac{2 \cdot r \cdot h \cdot l_g}{w \cdot D}\right)}{l_g + h} \qquad C_2 := C_t$$

$$C_3(r, l_g) := C_1(r, l_g) - \frac{2 \cdot r \cdot h}{w \cdot D} \qquad C_4(r, l_g) := \frac{-r}{w \cdot D} \cdot h^2 + C_1(r, l_g) \cdot h + C_t$$

$$C_c(y, r, l_g) := \frac{-r}{w \cdot D} \cdot y^2 + C_1(r, l_g) \cdot y + C_t$$

$$C_g(y, r, l_g) := C_3(r, l_g) \cdot y + C_4(r, l_g)$$

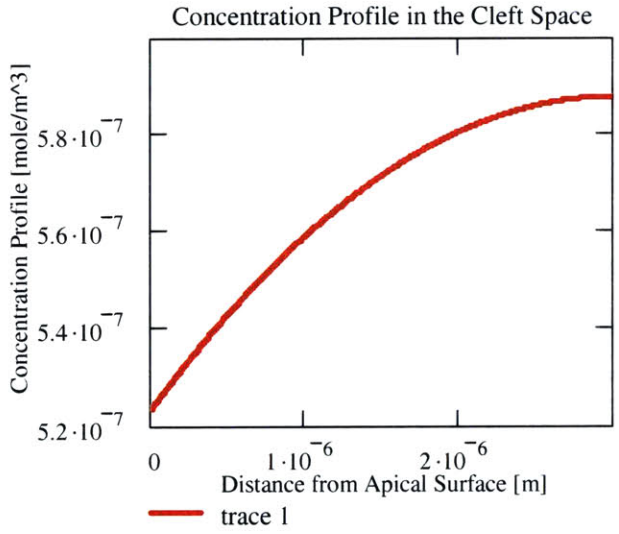

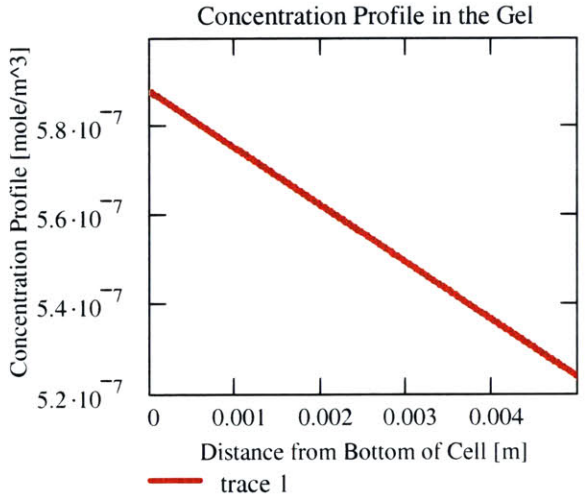

Diffusion + Convection

$$w_2(u_g,u_c) := -(b+l) + \sqrt{(b+l)^2 + \frac{u_g \cdot 4 \cdot l \cdot b}{u_c - u_g}}$$

$$C_6(u_g,u_c,l_g,r) := \frac{\frac{-2 \cdot r \cdot h}{w_2(u_g,u_c) \cdot u_c} + \frac{2 \cdot r \cdot D}{w_2(u_g,u_c) \cdot u_c \cdot u_g} \cdot \left(1 - e^{\frac{u_g \cdot l_g}{D}}\right)}{e^{\frac{u_c \cdot h}{D}} - 1 - \frac{u_c}{u_g} \cdot e^{\frac{u_c \cdot h}{D}} + \frac{u_c}{u_g} \cdot e^{\frac{u_c \cdot h}{D}} \cdot e^{\frac{u_g \cdot l_g}{D}}}$$

$$C_8(u_g,u_c,l_g,r) := \left(C_6(u_g,u_c,l_g,r) \cdot \frac{u_c}{u_g} \cdot e^{\frac{u_c \cdot h}{D}}\right) + \frac{2 \cdot r \cdot D}{w_2(u_g,u_c) \cdot u_g \cdot u_c}$$

$$C_5(u_g,u_c,l_g,r) := C_t - C_6(u_g,u_c,l_g,r)$$

$$C_7(u_g,u_c,l_g,r) := C_t - C_8(u_g,u_c,l_g,r) \cdot e^{\frac{u_g \cdot l_g}{D}}$$

$$C_{cc}(u_g,u_c,l_g,r,y) := C_5(u_g,u_c,l_g,r) + C_6(u_g,u_c,l_g,r) \cdot e^{\frac{u_c \cdot y}{D}} + \frac{2 \cdot r}{w_2(u_g,u_c) \cdot u_c} \cdot y$$

$$C_{cg}(u_g,u_c,l_g,r,y) := C_7(u_g,u_c,l_g,r) + C_8(u_g,u_c,l_g,r) \cdot e^{\frac{u_g \cdot y}{D}}$$

For the Large Gel (5mm) Region

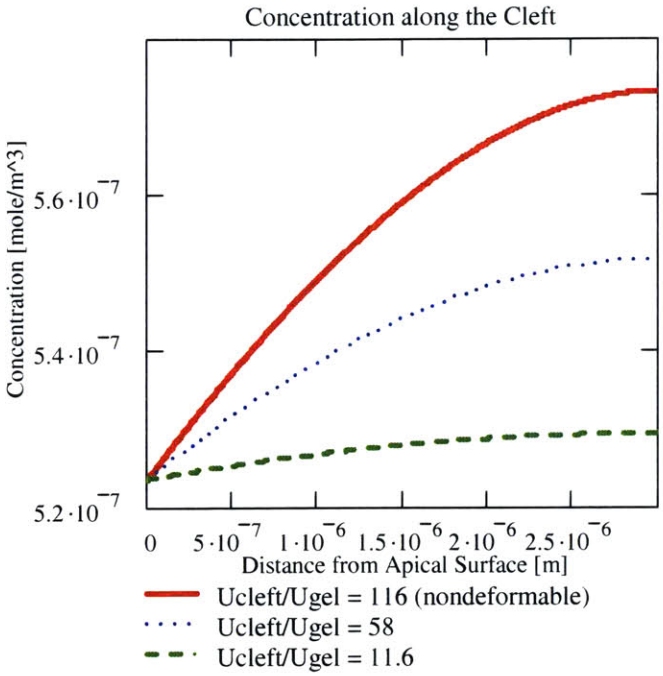

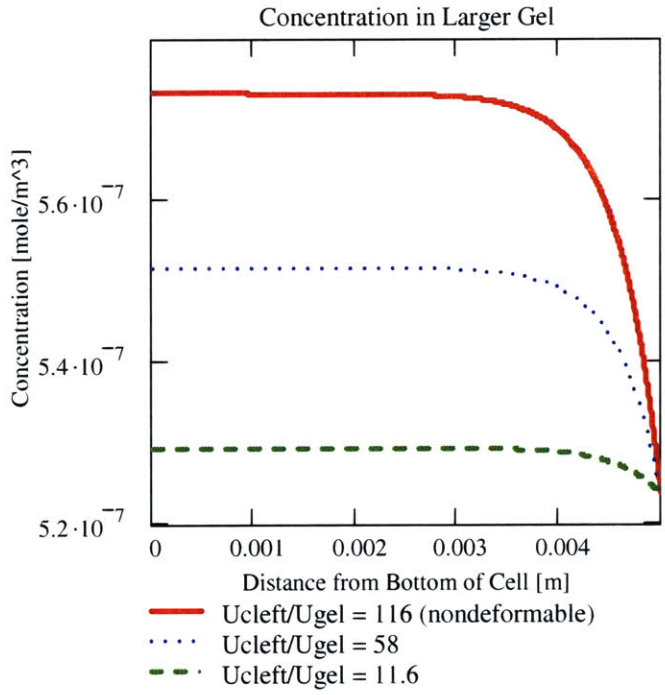

For the Smaller Gel (1mm) Region:

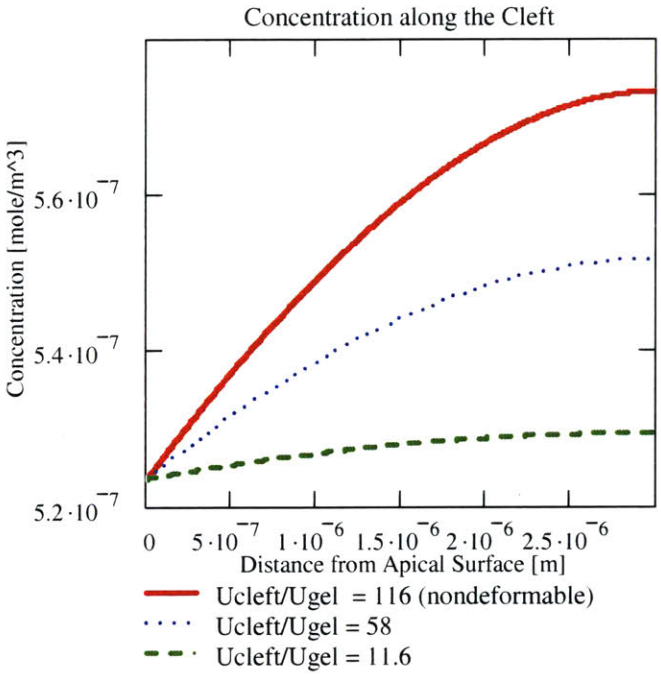

$C_t = 5.236\times 10^{-7}\ \frac{mol}{m^3}$

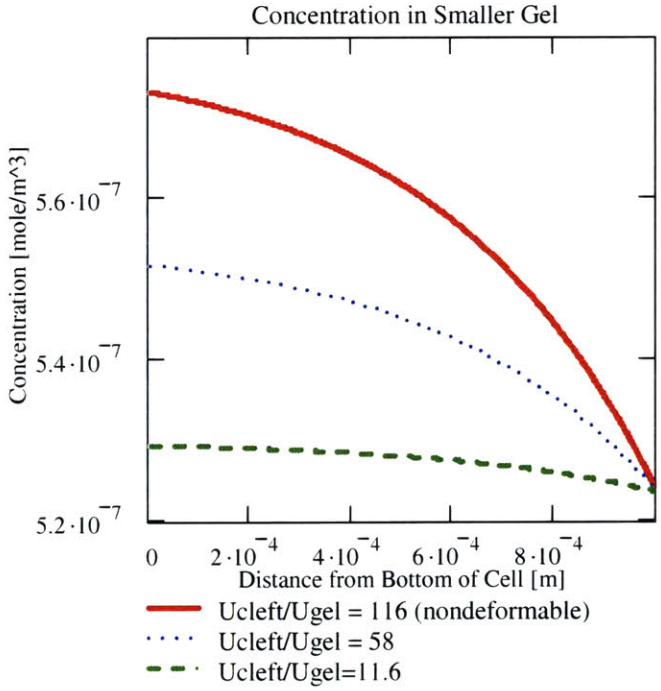

References

(1) Langer, R.; Vacanti, J. P. *Science* **1993**, *260*, 920-926.

(2) Risau, W. *Kidney Int.* **1998**, *54*, S3-S6.

(3) Risau, W.; Flamme, I. *Annu. Rev. Cell Dev. Biol.* **1995**, *11*, 73-91.

(4) Merks, R. M. H.; Brodsky, S. V.; Goligorksy, M. S.; Newman, S. A.; Glazier, J. A. *Dev. Biol.* **2006**, *289*, 44-54.

(5) Vailhe, B.; Vittet, D.; Feige, J. J. *Lab. Invest.* **2001**, *81*, 439-452.

(6) Damert, A.; Miquerol, L.; Gertsenstein, M.; Risau, W.; Nagy, A. *Development* **2002**, *129*, 1881-1892.

(7) Flamme, I.; Risau, W. *Development* **1992**, *116*, 435-439.

(8) Gulati, R.; Jevremovic, D.; Peterson, T. E.; Chatterjee, S.; Shah, V.; Vile, R. G.; Simari, R. D. *Circ. Res.* **2003**, *93*, 1023-1025.

(9) Risau, W. *Nature* **1997**, *386*, 671-674.

(10) Pepper, M. S.; Montesano, R. *Cell Differentiation and Development* **1990**, *32*, 319-328.

(11) Folkman, J.; Haudenschild, C. C.; Zetter, B. R. *Proc. Natl. Acad. Sci. U. S. A.* **1979**, *76*, 5217-5221.

(12) Clark, E. R.; Clark, E. L. *Am. J. Anat.* **1932**, *49*, 441-447.

(13) Folkman, J.; Haudenschild, C. *Nature* **1980**, *288*, 551-556.

(14) Ausprunk, D. H.; Folkman, J. *Microvasc. Res.* **1977**, *14*, 53-65.

(15) Ucuzian, A. A.; Greisler, H. P. *World J. Surg.* **2007**, *31*, 654-663.

(16) Nyalendo, C.; Michaud, M.; Gingras, D.; Beliveau, R. *EJC Suppl.* **2006**, *4*, 24-24.

(17) Kanda, S.; Miyata, Y.; Kanetake, H. *J. Biol. Chem.* **2004**, *279*, 4007-4016.

(18) Liu, Y. Q.; Senger, D. R. *FASEB J.* **2004**, *18*, 457-468.

(19) Pepper, M. S. *Arterioscler. Thromb. Vasc. Biol.* **2001**, *21*, 1104-1117.

(20) Kappel, A.; Ronicke, V.; Damert, A.; Flamme, I.; Risau, W.; Breier, G. *Blood* **1999**, *93*, 4284-4292.

(21) Koblizek, T. I.; Weiss, C.; Yancopoulos, G. D.; Deutsch, U.; Risau, W. *Curr. Biol.* **1998**, *8*, 529-532.

(22) Nicosia, R. F.; Nicosia, S. V.; Smith, M. *Am. J. Pathol.* **1994**, *145*, 1023-1029.

(23) Song, J.; Rolfe, B. E.; Hayward, I. P.; Campbell, G. R.; Campbell, J. H. *In Vitro Cell. Dev. Biol. -Anim.* **2000**, *36*, 600-610.

(24) Dye, J. F.; Lawrence, L.; Linge, C.; Leach, L.; Firth, J. A.; Clark, P. *Endothelium* **2004**, *11*, 151-167.

(25) Sieminski, A. L.; Hebbel, R. P.; Gooch, K. J. *Exp. Cell Res.* **2004**, *297*, 574-584.

(26) Sieminski, A. L.; Gooch, K. J. *Journal of Biomaterials Science-Polymer Edition* **2004**, *15*, 237-242.

(27) Bin Kim, J.; Stein, R.; O'Hare, M. J. *Breast Cancer Res. Treat.* **2004**, *85*, 281-291.

(28) Sieminski, A. L.; Gooch, K. J. *Biomaterials* **2000**, *21*, 2233-2241.

(29) Sieminski, A. L.; Was, A. S.; Kamm, R. D. *Mol. Biol. Cell* **2004**, *15*, 299A-299A.

(30) Sieminski, A. L.; Hebbel, R. P.; Gooch, K. J. *Tissue Eng.* **2005**, *11*, 1332-1345.

(31) Fisher, C.; Gilbertsonbeadling, S.; Powers, E. A.; Petzold, G.; Poorman, R.; Mitchell, M. A. *Dev. Biol.* **1994**, *162*, 499-510.

(32) Huang, H. D.; Kamm, R. D.; Lee, R. T. *Am. J. Physiol. -Cell Physiol.* **2004**, *287*, C1-C11.

(33) Lammerding, J.; Kamm, R. D.; Lee, R. T. *Ann. NY Acad. Sci.* **2004**, *1015*, 53-70.

(34) Iomini, C.; Tejada, K.; Mo, W. J.; Vaananen, H.; Piperno, G. *J. Cell Biol.* **2004**, *164*, 811-817.

(35) Chen, K. D.; Li, Y. S.; Kim, M.; Li, S.; Yuan, S.; Chien, S.; Shyy, J. Y. J. *J. Biol. Chem.* **1999**, *274*, 18393-18400.

(36) Li, S.; Kim, M.; Hu, Y. L.; Jalali, S.; Schlaepfer, D. D.; Hunter, T.; Chien, S.; Shyy, J. Y. J. *J. Biol. Chem.* **1997**, *272*, 30455-30462.

(37) Duncan, R. L.; Turner, C. H. *Calcif. Tissue Int.* **1995**, *57*, 344-358.

(38) Gupta, V.; Grande-Allen, K. J. *Cardiovasc. Res.* **2006**, *72*, 375-383.

(39) Ferri, A.; Grazi, E. *Biochem. J.* **1982**, *205*, 281-284.

(40) Chien, S. *American Journal of Physiology-Heart and Circulatory Physiology* **2007**, *292*, H1209-H1224.

(41) Li, S.; Huang, N. F.; Hsu, S. *J. Cell. Biochem.* **2005**, *96*, 1110-1126.

(42) Li, Y. S. J.; Haga, J. H.; Chien, S. *J. Biomech.* **2005**, *38*, 1949-1971.

(43) Shyy, J. Y.; Chien, S. *Circ. Res.* **2002**, *91*, 769-775.

(44) Sato, M.; Nagayama, K.; Kataoka, N.; Sasaki, M.; Hane, K. *J. Biomech.* **2000**, *33*, 127-135.

(45) Sato, M.; Ohshima, N.; Nerem, R. M. *J. Biomech.* **1996**, *29*, 461-467.

(46) Rutkowski, J. M.; Swartz, M. A. *Trends Cell Biol.* **2007**, *17*, 44-50.

(47) Ng, C. P.; Swartz, M. A. *Am. J. Physiol. -Heart Circul. Physiol.* **2003**, *284*, H1771-H1777.

(48) Ng, C. P.; Swartz, M. A. *Ann. Biomed. Eng.* **2006**, *34*, 446-454.

(49) Swartz, M. A.; Helm, C. E.; Fleury, M. E.; Shields, J. D.; Rutkowski, J. M.; Yong, C. *J. Vasc. Res.* **2006**, *43*, 25-25.

(50) Swartz, M. A.; Boardman, K. C. *FASEB J.* **2003**, *17*, A71-A71.

(51) Swartz, M. A.; Kaipainen, A.; Netti, P. A.; Brekken, C.; Boucher, Y.; Grodzinsky, A. J.; Jain, R. K. *J. Biomech.* **1999**, *32*, 1297-1307.

(52) Ng, C. P.; Swartz, M. A. *Am. J. Physiol. -Heart Circul. Physiol.* **2005**, *288*, H3016-H3016.

(53) Ng, C. P.; Helm, C. L. E.; Swartz, M. A. *Microvasc. Res.* **2004**, *68*, 258-264.

(54) Helm, C. L. E.; Fleury, M. E.; Zisch, A. H.; Boschetti, F.; Swartz, M. A. *Proc. Natl. Acad. Sci. U. S. A.* **2005**, *102*, 15779-15784.

(55) Fleury, M. E.; Boardman, K. C.; Swartz, M. A. *Biophys. J.* **2006**, *91*, 113-121.

(56) Semino, C. E.; Kamm, R. D.; Lauffenburger, D. A. *Exp. Cell Res.* **2006**, *312*, 289-298.

(57) Hernandez, R. Design and Fabrication of a New Bioreactor for Vascular Tissue Engineering, Massachusetts Institute of Technology, 2006.

(58) Wang, S.; Tarbell, J. M. *Arterioscler. Thromb. Vasc. Biol.* **2000**, *20*, 2220-2225.

(59) Helm, C. L. E.; Zisch, A.; Swartz, M. A. *Biotechnol. Bioeng.* **2007**, *96*, 167-176.

(60) Montesano, R.; Pepper, M. S.; Vassalli, J. D.; Orci, L. *J. Cell. Physiol.* **1987**, *132*, 509-516.